Published OnlineFirst October 12, 2012; DOI: 10.1158/0008-5472.CAN-12-0088

Cancer Research

NF-κB Activity Regulates Mesenchymal Stem Cell Accumulation at Tumor Sites

Ryosuke Uchibori, Tomonori Tsukahara, Hiroyuki Mizuguchi, et al.

Cancer Res 2013;73:364-372. Published OnlineFirst October 12, 2012.

Published OnlineFirst October 12, 2012; DOI: 10.1158/0008-5472.CAN-12-0088

Tumor and Stem Cell Biology

Cancer Research

NF-κB Activity Regulates Mesenchymal Stem Cell Accumulation at Tumor Sites

Ryosuke Uchibori[1], Tomonori Tsukahara[1], Hiroyuki Mizuguchi[4], Yasushi Saga[2], Masashi Urabe[1], Hiroaki Mizukami[1], Akihiro Kume[1], and Keiya Ozawa[1,3]

Abstract

Mesenchymal stem cells (MSC) accumulate at tumor sites when injected into tumor-bearing mice, perhaps offering cellular vectors for cancer-targeted gene therapy. However, the molecular mechanisms involved in MSC targeting the tumors are presently little understood. We focused on MSC–endothelial cell (EC) adhesion following TNF-α stimulation in an attempt to elucidate these mechanisms. Interestingly, stimulation of MSCs with TNF-α enhanced the adhesion of MSCs to endothelial cells *in vitro*. This adhesion was partially inhibited by blocking antibodies against vascular cell adhesion molecule-1 (VCAM-1) and very late antigen-4 (VLA-4). It is well known that TNF-α induces VCAM-1 expression via the NF-κB signaling pathway. Parthenolide has an anti-inflammatory activity and suppressed NF-κB activity by inhibition of IκBα phosphorylation after TNF-α stimulation and strongly inhibited TNF-α–induced VCAM-1 expression on MSCs. *In vivo* imaging using luciferase-expressing MSCs revealed that the bioluminescent signal gradually increased at tumor sites in mice injected with untreated MSCs. In contrast, we observed very weak signals at tumor sites in mice injected with parthenolide-treated MSCs. Our results suggest that NF-κB activity regulates MSC accumulation at tumors, by inducing VCAM-1 and thereby its interaction with tumor vessel endothelial cells. These findings have implications for the ongoing development of efficient MSC-based gene therapies for cancer treatment. *Cancer Res; 73(1); 364–72. ©2012 AACR.*

Introduction

Mesenchymal stem cells (MSC) are nonhematopoietic stem cells with high-proliferative potency and have the ability to differentiate into multiple lineages. They are detected in several adult and fetal tissues, including bone marrow, adipose tissue, and umbilical cord blood. MSCs have generated a great deal of interest in their potential use in regenerative medicine due to their ability to migrate to damaged tissues and to produce cytokines. Furthermore, MSCs can be easily genetically modified with viral vectors to be used as novel cellular vehicles in gene therapy protocols. MSCs are also used to treat severe acute GVHD, because they accumulate at inflammatory lesions and have immunomodulatory activity.

Interestingly, recent studies indicated that MSCs also have the ability to accumulate in tumors. Therefore, they can be used as cellular vehicles for cancer-targeted gene therapy. Intravenous injection of engineered MSCs expressing IFN-β was reported to inhibit the growth of melanoma pulmonary metastasis (1) and breast cancer (2) in mice and also prolonged the survival of mice with glioma xenografts (3). Furthermore, interleukin (IL)-12, which improves immune surveillance against cancer cells (4), and chemokine CX3CL1 (fractalkine), which is able to activate T cells and natural killer (NK) cells (5), were used as therapeutic molecules. We have also shown that retrovirus vector–producing MSCs also effectively inhibit tumor growth (6). In this context, treatment has been developed using retroviral vectors expressing the thymidine kinase of herpes simplex virus combined with the prodrug ganciclovir.

The ability of MSCs to specifically localize the multiple tumors, makes them extremely attractive for targeted cancer therapy. The most likely cause of preferential migration was considered to be the release of chemotactic gradients from tumor tissues. MSCs have a variety of chemokine and cytokine receptors and respond functionally to ligands *in vitro*. Tumors are known to produce a large amount of chemokines and cytokines, which could serve as ligands for the receptors on MSCs (7). Therefore, the mechanism of MSC accumulation at the site of tumors seems to be based on their migratory ability. Nevertheless, although various growth factors and chemokines, such as platelet-derived growth factor (PDGF), hepatocyte growth factor (HGF), and stromal cell–derived factor-1α (SDF-1α) may be involved, the detailed molecular mechanisms of MSC accumulation at tumors are poorly understood.

Authors' Affiliations: [1]Division of Genetic Therapeutics, Center for Molecular Medicine; [2]Department of Obstetrics and Gynecology; [3]Division of Hematology, Department of Medicine, Jichi Medical University, Tochigi; and [4]Department of Biochemistry and Molecular Biology, Osaka University, Osaka, Japan

Note: Supplementary data for this article are available at Cancer Research Online (http://cancerres.aacrjournals.org/).

Corresponding Author: Keiya Ozawa, Division of Genetic Therapeutics, Center for Molecular Medicine, Jichi Medical University, 3311-1 Yakushiji, Shimotsuke, Tochigi 329-0498, Japan. Phone: 81-285-58-7402; Fax: 81-285-44-8675; E-mail: kozawa@jichi.ac.jp

doi: 10.1158/0008-5472.CAN-12-0088

Published OnlineFirst October 12, 2012; DOI: 10.1158/0008-5472.CAN-12-0088

In the present study, we focused on MSC–endothelial cell (EC) adhesion following TNF-α stimulation in an attempt to elucidate the mechanism of MSC accumulation at tumors.

Materials and Methods

Cell culture

Bone marrow–derived human MSCs (Lonza Walkersville, Inc.) were cultured in mesenPRO RS medium (Invitrogen). HEK293-derived AD-293 cells (Stratagene), human embryonic fibroblasts WI-38 (RIKEN BRC), human colon adenocarcinoma cell lines SW480 (Cell Resource Center for Biomedical Research Institute of Development, Aging and Cancer, Tohoku University, Miyagi, Japan), and SW480/RFP that was generated by transduction of SW480 with red fluorescent protein-expressing retrovirus vectors (RV-RFP), were grown in Dulbecco's Modified Eagle's Medium (DMEM)/F-12 medium (Invitrogen) supplemented with 10% FBS, 100 U/mL penicillin, and 100 μg/mL streptomycin (P/S). Human endothelial progenitor cells (ApproCell Inc.) were cultured in endothelial progenitor cells grown medium (ApproCell Inc.). Human colon adenocarcinoma cell lines Colo205 (Cell Resource Center for Biomedical Research Institute of Development, Aging and Cancer Tohoku University) and Colo205/RFP that was generated by transduction with RV-RFP, were grown in RPMI medium (Invitrogen) supplemented with FBS and P/S. All cultures were kept in an incubator at 37°C and 5% CO_2.

Adenoviral vectors

Adenoviral vectors expressing a GFP were constructed by an improved *in vitro* ligation method (8, 9). The shuttle plasmid pHMCA5-GFP contains a CA promoter (a β-actin promoter/CMV enhancer with a β-actin intron), *GFP* gene, and a bovine growth hormone (BGH) polyadenylation signal, all of which are flanked by I-CeuI and PI-SceI restriction sites. I-CeuI/PI-SceI–digested pHMCA5-GFP was ligated with I-CeuI/PI-SceI–digested pAdHM4, resulting in pAdHM4-CAGFP. pAdHM41-K7-CAGFP was constructed by ligation of I-CeuI/PISceI–digested pHMCA5-GFP with I-CeuI/PI-SceI–digested pAdHM41-K7 (10). Viruses (Ad5-GFP and AdK7-GFP) were generated by transfection of PacI-digested pAdHM4-CAGFP and pAdHM41-K7-CAGFP, respectively, into AD-293 cells with SuperFect (Qiagen) according to the manufacturer's instructions. Each virus was purified by $CsCl_2$ step gradient ultracentrifugation followed by $CsCl_2$ linear gradient ultracentrifugation. Virus particles and biologic titers of each vector preparation were determined as described by Mittereder and colleagues (11). We also created Ad vectors expressing luciferase (Luc) using the shuttle plasmid pHMCA5-Luc, which contains the *Luc* gene derived from pELuc-test (Toyobo Co. Ltd.). MSCs and fibroblasts were seeded in culture plates or flasks at a density of 1×10^4 cells/cm^2, and the next day the cells were treated with each adenovirus vector for 1.5 hours. The medium containing the vectors was removed and replaced with fresh medium.

Animal models

All animal experiments were approved by the Jichi Medical University (Tochigi, Japan) ethics committee and carried out in accordance with the NIH Guide for the Care and Use of Laboratory Animals. To create tumor-bearing mice, SW480/RFP cells (3×10^6) were subcutaneously inoculated into 4- to 6-week-old male Balb/c nu/nu mice (Clea Japan Inc.). The mice were used for experiments 7 days after inoculation.

Immunohistochemistry

Cultured MSCs and fibroblasts were transduced with AdK7-GFP at a concentration of 3,000 virus particles per cell (vp/cell). Two days after transduction, cells were injected into the left ventricular cavities (1×10^6, day 0) of tumor-bearing mice. Mice were sacrificed on day 4, and 7-μm serial cryosections from frozen tissues were processed. Immunohistochemistry was conducted with fluorescein isothiocyanate (FITC)-conjugated anti-GFP antibody (ab6662; Abcam Inc.) on tumor cryosections to detect MSCs or fibroblasts. Nuclei were stained with 4′,6-diamidino-2-phenylindole (DAPI; Vector Laboratories, Inc.). Images were obtained with a fluorescence microscope (BZ-9000; Keyence). SW480/RFP cells (3×10^6) were subcutaneously inoculated into 4- to 6-week-old male Balb/c nu/nu mice. Mice were sacrificed on day 11, serial sections from tumor tissues were processed. Immunohistochemistry was conducted with anti-mouse CD34 monoclonal antibody (MEC14.7; GeneTex Inc.) on tumor section to detect tumor blood vessels. Histofine Simple Stain Mouse MAX PO (Nichirei Biosciences, Inc.) was used as a horseradish peroxidase–conjugated secondary antibody, and 3,3′-diaminobenzidine (DAB) solution was used for brown color development. Sections were then counterstained with Hematoxylin (Wako Pure Chemical Industries, Ltd.). Images were obtained with a fluorescence microscope (BZ-9000).

In vivo imaging of homing ability to tumors

Cultured MSCs and fibroblasts were transduced with AdK7-Luc at a concentration of 3,000 and 680 vp/cell, respectively. Two days after transduction, cells were injected into the left ventricular cavities (1×10^6, day 0) of tumor-bearing mice, and then optical bioluminescence imaging was conducted to periodically trace the cells using an *in vivo* imaging system (IVIS; Xenogen). To detect bioluminescence from MSCs or fibroblasts, the reporter substrate D-luciferin (Ieda Chemical Co., Ltd.) was injected into the mouse peritoneum (75 mg/kg body weight) for scanning. The luminescent intensity at tumor sites was analyzed using Living Image software (Xenogen).

In vitro migration assays

Cultured MSCs or fibroblasts were serum-starved for 12 hours. One hundred microliters of tumor conditioning medium (CM), or serum-free medium supplemented with PDGF-BB (10 ng/mL), HGF (30 ng/mL), fibroblast growth factor-β (FGF-β; 20 ng/mL), SDF-1α (150 ng/mL), VEGF-A (25 ng/mL), or monocyte chemoattractant protein-1 (MCP-1; 100 ng/mL) was added to the lower wells of migration chambers (8-μm pore size; Neuro Probe, Inc.); MSCs or fibroblasts (4×10^4) were added to the upper wells. All recombinant proteins were purchased from R&D systems Inc.. Medium alone (DMEM/F-12) was used as a negative control and treatment with 30% FBS was the positive control. After incubation for 24 hours at

Published OnlineFirst October 12, 2012; DOI: 10.1158/0008-5472.CAN-12-0088

37°C, cells were labeled with CyQUANT NF dye, and cells attached to the lower surface of the filters were detached with trypsin. Fluorescent intensity was measured using a fluoroscan, and the number of adherent cells was quantified using a standard curve constructed by a known number of cells.

Flow cytometric analysis of adhesion molecules

Cultured MSCs, fibroblasts or endothelial cells were stimulated with TNF-α and harvested by trypsinization. Cell aliquots were incubated with FITC-conjugated monoclonal antibodies (BD) against vascular cell adhesion molecule-1 (VCAM-1), CD49d, CD29 (Integrin-β1), and analyzed by flow cytometry (FACScan; BD Biosciences). For each analysis, an aliquot of cells was also stained with isotype control immunoglobulin G (IgG)–conjugated to FITC as a negative control.

Assay for TNF-α produced in tumor-bearing mice

SW480/RFP (3×10^6) cells were subcutaneously inoculated into nude mice. Seven days after inoculation, mice were anesthetized with an overdose of isoflurane inhalation. The blood was collected and allowed to coagulate overnight on ice. After centrifugation of the samples ($2,000 \times g$, 30 minutes, 4°C), the serum was removed and stored at −70°C. Tumor, spleen, and liver tissues were homogenized in 1.5 mL of α-minimum essential medium using a tissue homogenizer. The homogenates were then centrifuged ($2,000 \times g$, 30 minutes, 4°C), and the supernatant was removed and recentrifuged ($14,000 \times g$, 30 minutes, 4°C). Serum and supernatants from tissue homogenates were kept at −70°C until use. TNF-α was assayed using a commercially available ELISA kit (mouse TNF-α Instant ELISA; Bender MedSystems) according to the manufacturer's protocols.

***In vitro* adhesion assays**

For adhesion assays, endothelial cells (at 4 passages) were cultured to confluence on fibronectin-coated 96-well plates (20 ng/mL; Sigma-Aldrich, Inc.) and treated with TNF-α (10 ng/mL) for 12 hours before assaying. MSCs and fibroblasts were treated with TNF-α (10 ng/mL) 12 hours before the adhesion assays and incubated with isotype control IgG or anti-VCAM-1 or very late antigen-4 (VLA-4; 10 μg/mL) monoclonal antibodies (mAb) for 1 hour. Cells were labeled with CyQUANT NF dye, and 1×10^4 cells were seeded onto endothelial cells. After 30 minutes of incubation at 37°C, wells were washed thoroughly 3 times with PBS to remove nonadherent cells. Fluorescent intensity was measured using a fluoroscan, and the number of adherent cells was quantified using a standard curve constructed by a known number of cells. In some experiments, MSCs and fibroblasts were pretreated for adhesion studies with one of the following substances: TNF-α (10 ng/mL), anti-VCAM-1 antibody (mouse monoclonal anti-rat, clone 5F10, 10 μg/mL, Eurogentec), or anti-VLA-4 antibody (mouse monoclonal anti-rat, clone 1A29, 10 μg/mL, Research Diagnostics).

Parthenolide treatment of MSCs

Parthenolide (Biomol) was reconstituted in dimethyl sulfoxide (DMSO; Sigma-Aldrich, Inc.) to a stock concentration of 0.4 mol/L and subsequently diluted in PBS. MSCs were treated with parthenolide (5 μmol/L) for 6 hours before experiments. To assess the effect of parthenolide treatment of transgene expression, cells were reseeded into 96-well plates, and luciferase assays were conducted using luciferase-expressing MSCs. Cell viability after parthenolide treatment was also examined with Cell Proliferation Kit II [2,3-bis[2-methoxy-4-nitro-S-sulfophenynl]H-tetrazolium-5 carboxanilide inner salt (XTT); Roche Diagnostics GmbH] according to the manufacturer's instructions.

Western blotting

Western blot analysis was conducted to measure the NF-κB pathways. Next, MSCs were pretreated with parthenolide or vehicle (DMSO) for 6 hours, and then cultured with TNF-α (10 ng/mL) for 3 minutes. Cells were lysed in radioimmunoprecipitation assay (RIPA) buffer containing protease inhibitor (Pierce Biotechnology). Protein extracts were electrophoresed on a 4% to 12% Bis–Tris gel (Invitrogen), and transferred to polyvinylidene difluoride (PVDF) membranes. Membranes were incubated in PVDF blocking reagent (TOYOBO), and then incubated with primary antibodies against the following proteins: IκBα, phospho-IκBα (Ser32), NF-κB p65, phospho-NF-κB p65 (Ser536), and α-tublin (Cell Signaling Technology), followed by incubation with horseradish peroxidase-conjugated goat anti-rabbit IgG or -mouse IgG1 secondary antibody, and detected using a Western blotting detection system (GE Healthcare).

Immunocytochemistry

To visualize p65 nuclear translocation, MSCs were pretreated with parthenolide or vehicle (DMSO) for 6 hours and then cultured with TNF-α (10 ng/mL) for 20 minutes. Cells were fixed with 4% fomaline and permiabilized with Triron-X 100. After washing with PBS, slides were incubated with rabbit anti-p65 antibody (Cell Signaling Technology), followed by incubation with Alexa Fluor 488–conjugated goat anti-rabbit IgG secondary antibody. The actin cytoskeleton was stained with Alexa Fluor 546–conjugated phalloidin (Invitrogen); nuclei were stained with 1,5-bis{[2-(di-methylamino) ethyl]amino}-4,8-dihydroxyanthracene-9,10-dione (DRAQ)-5 dye (Invitrogen). Cells were examined using Keyence BZ-9000.

Results

***In vivo* imaging of MSC accumulation in tumors**

We used bone marrow–derived human MSCs, which expressed characteristic phenotypic markers for MSCs and differentiated into adipocyte, osteocyte, and chondrocyte under specific culture conditions (Supplementary Fig. S1). Then, fiber-modified adenovirus vectors (AdK7) were used for efficient transduction of MSCs and fibroblasts in this study. When the cells were transduced with GFP-expressing AdK7 vectors at a density of 3,000 vp/cell, transduction efficiency was almost 100% (Supplementary Fig. S2A and S2B). The bioluminescent intensity of MSCs transduced with luciferase-expressing Ad vectors at 3,000 vp/cell was equal to that of fibroblasts transduced at 680 vp/cell (Supplementary Fig. S2C). Mice injected with GFP-expressing MSCs or fibroblasts were sacrificed 4 days after injection for immunohistochemical analysis.

Published OnlineFirst October 12, 2012; DOI: 10.1158/0008-5472.CAN-12-0088

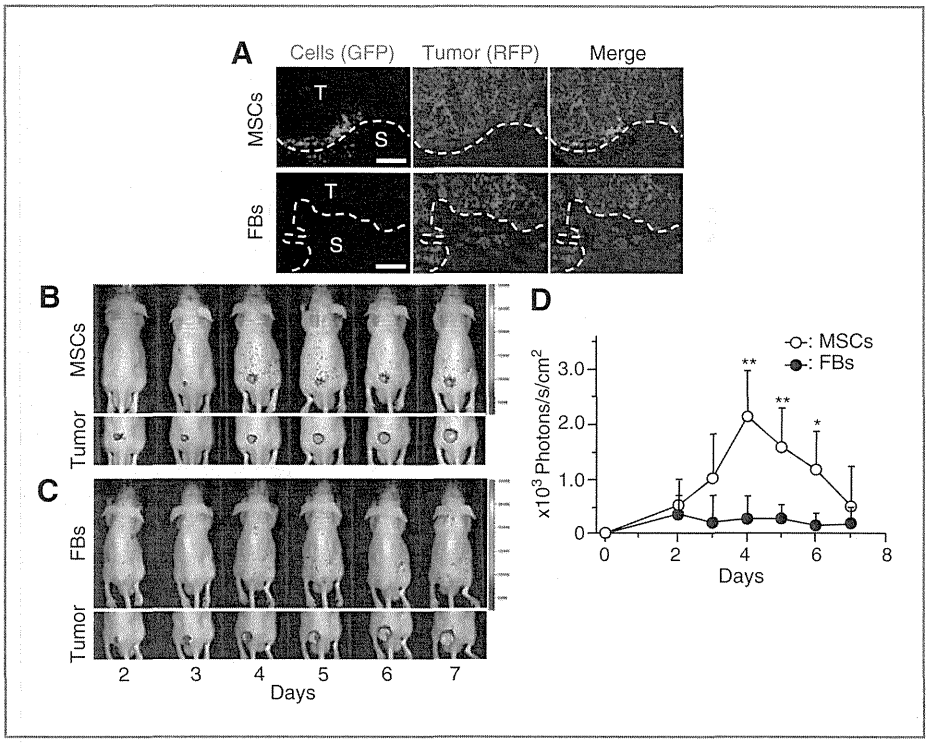

Figure 1. Tumor homing ability of MSCs *in vivo*. A, subcutaneous tumors were induced by injection of SW480/RFP cells (3×10^6) in nude mice (day 0). Cultured MSCs or fibroblasts were transduced with GFP-expressing adenovirus vectors 2 days before injection (day 5) and were injected into the left ventricular cavity (1×10^6, day 7). Mice were sacrificed on day 11, and immunohistochemistry was conducted with anti-GFP antibody on tumor cryosections to detect MSCs or fibroblasts. Top, fluorescent microscopy view of MSC detection; MSCs (left), RFP-labeled tumor cells (center), nucleic staining with DAPI and merge (right). Bottom, fluorescent microscopy view of fibroblast detection; fibroblasts (left), RFP-labeled tumor cells (center), nucleic staining with DAPI and merge (right). Data shown are from 1 representative experiment of 3 carried out. Scale bar, 100 μm. S, stroma; T, tumor. B, luciferase-expressing MSCs were injected into tumor-bearing mice via the left ventricular cavity (1×10^6, day 7). Optical bioluminescence imaging was conducted to periodically trace the cells using IVIS. Top, biodistribution of MSCs as detected by luminescence. Bottom, tumor site detected by red fluorescence. Data shown are from 1 representative experiment of 8 carried out. C, luciferase-expressing fibroblasts were injected into tumor-bearing mice and IVIS imaging was conducted as described earlier. Top, biodistribution of fibroblasts indicated by luminescence. Bottom, tumor site indicated by red fluorescence. Data shown are from 1 representative experiment of 7 carried out. D, bioluminescent intensity at tumor sites was quantified using analysis software. The data are expressed as mean ± SD ($n = 8$ for MSCs and $n = 7$ for fibroblasts). *, $P < 0.05$; **, $P < 0.01$ compared with fibroblasts at the same time.

MSCs identified with anti-GFP antibody were detected in the boundaries of tumors and tumor stroma. However, we found no GFP-positive fibroblasts in the tumor tissues (Fig. 1A). We also used bioluminescence imaging to quantitatively investigate the tumor tropism of MSCs. We injected luciferase-expressing MSCs or fibroblasts into mice through the left ventricular cavity, and then conducted optical bioluminescence imaging to periodically trace the cells using IVIS. In mice injected with luciferase-expressing MSCs, optical bioluminescence at tumor sites became pronounced over time (Fig. 1B), and signal intensity gradually increased (Fig. 1D). In contrast, we observed no signal at the tumor sites in mice injected with luciferase-expressing fibroblasts (Fig. 1C and D).

In vitro migration assays

We analyzed the effects of several growth factors (specifically PDGF-BB, HGF, and VEGF), chemokines (specifically MCP-1 and SDF-1α), and SW480 culture–conditioned medium on MSC and fibroblast migration. These factors are commonly expressed in tumor tissues, and are thought to be potential mediators of MSC tropism. We also used serum-free medium as a negative control and medium containing 30% FBS as a positive control. Migration was quantified by direct labeling and counting of cells by a fluorometer (Fluoroskan Ascent FL; Thermo Labsystems). Exposure to PDGF, HGF, or conditioned medium from SW480 cells stimulated significant MSC migration, whereas VEGF and SDF-1α had no significant effect as compared with serum-free medium (Fig. 2). We compared the migration capacity of MSCs and fibroblasts, the factors that attracted MSCs also induced migration of fibroblasts. Rather, it seems that fibroblasts were more strongly attracted to these factors than MSCs.

In vitro adhesion assays

The tumors generated in mice in this study strongly induced tumor stroma with defined blood vessels, and MSCs specifically accumulated in this stroma (Fig. 3A). Therefore, we propose a hypothesis as follows: factors, as indicated in Fig. 2, attract both MSCs and fibroblasts to the tumor microenvironment, but importantly, MSCs significantly adhere to endothelial cells as

Published OnlineFirst October 12, 2012; DOI: 10.1158/0008-5472.CAN-12-0088

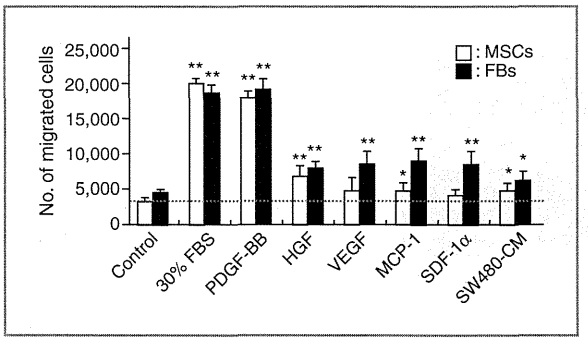

Figure 2. Migratory capacity of MSCs and fibroblasts (FB) in response to growth factors, chemokines, and conditioned medium from SW480 cells. MSCs or fibroblasts were serum-starved for 12 hours. Cells (4×10^4) were added to upper wells of migration chambers. Then, tumor conditioning medium, serum-free medium supplemented with PDGF-BB (10 ng/mL), HGF (30 ng/mL), SDF-1α (150 ng/mL), VEGF-A (25 ng/mL), or MCP-1 (100 ng/mL) were added to the lower wells. Treatment with medium alone (DMEM/F-12) was used as a negative control and treatment with 30% FBS was used as the positive control. The contents of the upper wells and lower wells were separated by polycarbonate filters (8 μm). The data are expressed as mean ± SD ($n = 8$ per cell type). Values are presented as mean ± SE. *, $P < 0.05$ and **, $P < 0.01$ compared with each control.

compared with fibroblasts. Therefore, only MSCs migrate and accumulate at tumor sites via blood vessels in tumor stroma. We speculated that inflammatory cytokines (specifically TNF-α) are required for induction of adhesion molecule expression. First, we measured TNF-α levels in tumor tissues by ELISA. The TNF-α level is significantly higher in tumor tissues as compared with liver and spleen (Fig. 3B). Similar results were also observed in another experiments using Colo205 tumor cells (Supplementary Fig. S3). Then, we assessed the expression of adhesion molecules on endothelial cells, MSCs, and fibroblasts by fluorescence-activated cell sorting analysis. After TNF-α stimulation, endothelial cells and MSCs significantly expressed adhesion molecules including VCAM-1 and VLA-4, compared with fibroblasts (Fig. 3C). We also examined the *in vitro* adhesion of MSCs to endothelial cells. MSCs effectively adhered to endothelial cells as compared with fibroblasts (Fig. 3D). Furthermore, this adhesion was partially inhibited by blocking antibodies against VCAM-1 and VLA-4.

Effects of parthenolide on MSC migration and adhesion

We propose a hypothesis that if TNF-α–induced VCAM-1 expression is inhibited, MSC accumulation at tumors is also attenuated. It is well known that TNF-α induces VCAM-1 expression through the NF-κB signaling pathway. We used parthenolide, a sesquiterpene lactone that occurs naturally in the Feverfew plant. Although parthenolide has several biologic activities, we focused on its suppressive effect on NF-κB activity. At first, there were no differences in migratory capacity toward growth factors or chemokines with or without parthenolide treatment (Fig. 4A). Next, we assessed the inhibitory effect of parthenolide on NF-κB activity: MSCs were pretreated for 6 hours, and then were stimulated with TNF-α for 3 minutes. Parthenolide suppressed p65 nuclear translocation through the inhibition of IκBα phosphorylation (Fig. 4B and C) and strongly inhibited the TNF-α–induced VCAM-1 expression on MSCs (Fig. 4D). Consequently, and MSC–EC adhesion was strongly inhibited by parthenolide treatment similarly to anti-VCAM-1 blocking antibody (Fig. 4E).

***In vivo* imaging of parthenolide-treated MSCs**

First, we examined the effect of parthenolide treatment on transgene expression and cell viability. There were no significant effects on transgene expression and cell viability after parthenolide treatment (Fig. 5A and B). Next, we conducted *in vivo* imaging using IVIS. We observed definite bioluminescence at tumor sites in the mice injected with untreated MSCs (Fig. 5C), and bioluminescent intensity was gradually increased (Fig. 5E), as indicated earlier (Fig. 1B). In contrast, we could not observe definite accumulation at the tumor sites in mice injected with parthenolide-treated MSCs (Fig. 5D and E). Similar results were also obtained by experiments using Colo205 tumor-bearing mice (Supplementary Fig. S4).

Discussion

In this study, we showed that MSC accumulation at tumor sites would be related not only to migratory capacity toward growth factors and chemokines, but also to MSC–EC adhesion following activation by TNF-α. We further showed that NF-κB activity regulates MSC accumulation at tumor sites through the induction of VCAM-1 expression and the resultant interaction with tumor blood vessel endothelial cells.

It is thought that MSCs are mobilized into action following tissue damage, such as injury or inflammation typically accompanied by the release of inflammatory cytokines from the damaged tissues, leading to the recruitment of MSCs to the target. Tumors have a microenvironment consisting of large numbers of inflammatory cells (12). This microenvironment promotes the recruitment of MSCs via various soluble factors secreted by the tumor and inflammatory cells, including EGF, VEGF-A, FGF, PDGF, SDF-1α, IL-8, IL-6, granulocyte colony-stimulating factor (G-CSF), granulocyte-macrophage colony-stimulating factor (GM-CSF), MCP-1, HGF, TGF-β1, and urokinase-type plasminogen activator (uPA; ref. 13). However, in our experimental settings, although systemically injected MSCs accumulated at the tumors, subcutaneously injected MSCs did not (data not shown). We also compared the migration capacity of MSCs and fibroblasts toward growth factors and chemokines *in vitro*. Rather, it seems that fibroblasts were more strongly attracted to these factors than MSCs. Our results suggest that the mechanism of MSC accumulation cannot be explained solely by cytokine-mediated migration. Therefore, we need different viewpoints to clarify the mechanism.

The tumors generated in this study strongly induced tumor stroma with large numbers of blood vessels, and MSCs in particular accumulated in the boundaries between the tumors and tumor stroma. Furthermore, MSC accumulation at the site of the tumors was observed only when cells were injected via the left ventricular cavity. Therefore, we focused on MSC–EC adhesion to elucidate the mechanisms involved.

It has previously been reported that the interaction of MSCs with the vascular endothelium resembles leukocyte chemotaxis (14). To analyze these interactions, we referred to a model

Published OnlineFirst October 12, 2012; DOI: 10.1158/0008-5472.CAN-12-0088

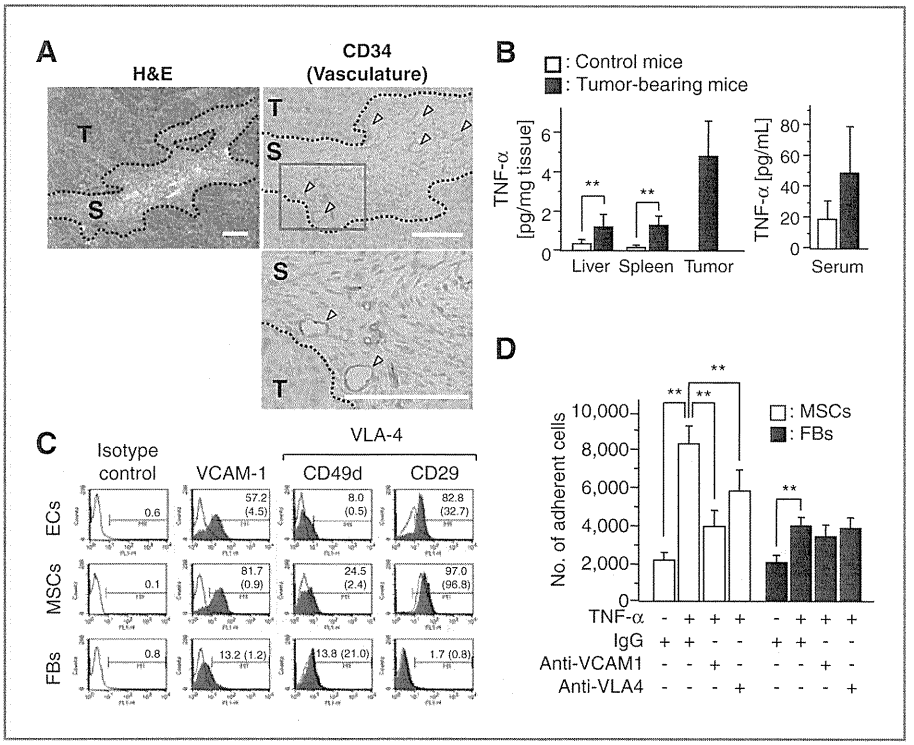

Figure 3. A, sections represent hematoxylin and eosin (H&E) staining (top left), the $CD34^+$ blood vessels/endothelial cells in tumor tissues (top right), the high-power field of view (bottom). Data shown are from 1 representative experiment of 3 carried out. Scale bar, 100 μm. S, stroma; T, tumor. B, specimens of tumor, liver, spleen, and blood were collected from control and tumor-bearing mice. TNF-α levels in tissue homogenates and serum were assayed by ELISA. *, $P < 0.05$; **, $P < 0.01$. C, MSCs, endothelial cells (EC), and fibroblasts were cultured with TNF-α (10 ng/mL) for 6 hours. Cells were labeled with FITC-conjugated antibodies and analyzed by flow cytometry (filled histogram). Rat isotype antibodies IgG1 and IgG2a served as respective controls (open histograms). Values represent the percentage of positive cells after TNF-α stimulation, and values in parentheses represent the percentage of positive cells without TNF-α stimulation. D, endothelial cells were cultured to confluence on fibronectin-coated 96-well plates. Then, MSCs or fibroblasts (1×10^4) were added to cultured endothelial cells. MSCs and endothelial cells were pretreated with the following substances: TNF-α (10 ng/mL), anti-VCAM-1, VLA-4 (10 μg/mL), or isotype control IgG. Values are mean ± SD. **, $P < 0.01$ ($n = 6$ per cell type).

that has been proposed for endothelial cell regulation of leukocyte infiltration in inflammatory tissues. Leukocyte-endothelial adhesion involves dynamic interactions between leukocytes and endothelial cells, and involves multiple steps. These steps must be precisely orchestrated to ensure a rapid response with minimal damage to healthy tissue (15). Interactions between leukocytes and the endothelium are mediated by several families of adhesion molecules, each of which participates in a different phase of the process. The surface expression and activation of these molecules during an inflammatory response is tightly controlled under normal conditions. Inflammatory cytokines including IL-1 and TNF-α involve induction of adhesion molecules. In our experimental settings, although other inflammatory cytokine levels including IL-1 and IL-6 were low (data not shown), significant production of TNF-α was observed. We do not clearly know the source of TNF-α in the tumor at this time, and that our *in vitro* data only suggest that the stroma is the primary source.

As we expected, TNF-α enabled MSCs to adhere to endothelial cells through induction of the expression of adhesion molecules, including VCAM-1 and VLA-4. It is generally considered that VCAM-1 on activated endothelium interacts with the VLA-4 on the leukocyte in the model of leukocyte–endothelial cell adhesion. At first, we speculated that VLA-4 on MSCs plays the same important role as leukocytes. Although both VCAM-1 and VLA-4 on endothelium were efficiently induced by TNF-α stimulation, TNF-α–induced expression of VCAM-1 on MSCs is much stronger than that of VLA-4. Furthermore, MSC–EC adhesion was more effectively inhibited by anti-VCAM-1 antibody as compared with the anti-VLA-4 antibody. On the basis of these results, although VLA-4 on MSC have also related to the MSC-EC adhesion, we thought that VCAM-1 on MSC has more important implications for this adhesion. Once MSCs circulate in the bloodstream, adhesion to endothelial cells is the first step in accumulation in tumors. TNF-α exerts its biologic functions through activating the NF-κB signaling pathway. NF-κB is a major cell survival signal that is antiapoptotic. MSC accumulation was significantly decreased through parthenolide inhibition of NF-κB activity. Although several studies have shown that mitogen-activated protein kinase (MAPK) phosphorylation by growth factors are involved in MSC migration (16, 17), parthenolide did not inhibit MAPK phosphorylation (data not shown). Therefore, at least parthenolide treatment did not affect in migration ability of

Published OnlineFirst October 12, 2012; DOI: 10.1158/0008-5472.CAN-12-0088

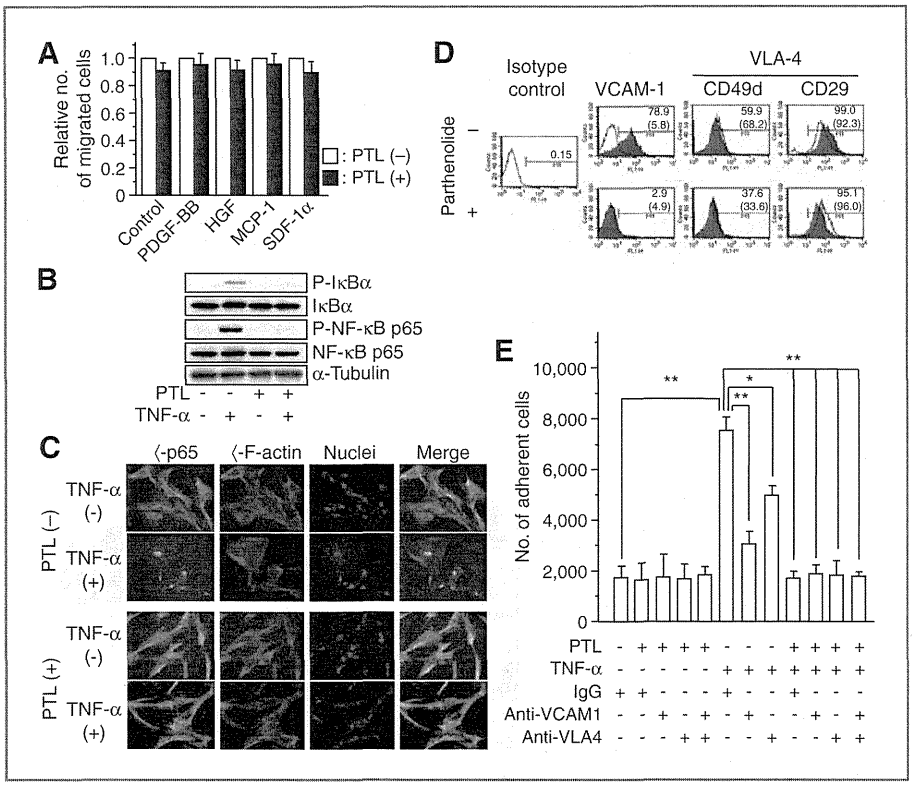

Figure 4. Effect of parthenolide (PTL) on MSC migration and adhesion. A, serum-starved and parthenolide-treated MSCs were added to the upper wells and serum-free medium supplemented with PDGF-BB (10 ng/mL), HGF (30 ng/mL), MCP-1 (100 ng/mL), or SDF-1α (150 ng/mL) was added to the lower wells. Treatment with medium alone (DMEM/F-12) was a negative control and treatment with 30% FBS was the positive control. Values are expressed by relative number of cells compared with respective controls (without pretreatment with parthenolide). B, to assess the inhibitory effect of parthenolide on NF-κB phosphorylation, parthenolide-treated MSCs were stimulated with recombinat TNF-α for 3 minutes, and cellular extracts were prepared for Western blotting. C, to monitor the inhibitory effect of parthenolide on NF-κB activation, immunofluorescent analysis of NF-κB p65 nuclear translocation was conducted as described in Materials and Methods with an Alexa Fluor 488–conjugated specific antibody (green). Actin filaments were labeled with Alexa Fluor 546–conjugated phalloidin (red); nuclei were stained with DRAQ-5 dye (blue). Objective magnification, ×40. D, effect of parthenolide treatment on TNF-α–induced expression of adhesion molecules was analyzed by flow cytometry. Parthenolide-treated MSCs were cultured with TNF-α (10 ng/mL) for 6 hours. Cells were labeled with FITC-conjugated antibodies and analyzed by flow cytometry (filled histogram). Rat isotype antibodies IgG1 and IgG2a served as respective controls (open histograms). Values represent the percentage of positive cells after TNF-α stimulation, and values in parentheses represent the percentage of positive cells without TNF-α stimulation. E, MSCs (1×10^4) were added to endothelial cells that had been cultured to confluence on fibronectin-coated 96-well plates. MSCs and endothelial cells were pretreated with the following substances: parthenolide (5 μmol/L), TNF-α (10 ng/mL), anti-VCAM-1, VLA-4 (10 μg/mL), or isotype control IgG. Values are expressed as mean ± SD ($n = 6$). *, $P < 0.05$ and **, $P < 0.01$.

MSCs toward growth factors from tumors in this experimental settings. Nevertheless, MSC accumulation was significantly decreased through parthenolide inhibition of NF-κB activity. We did not show histologic evidence in the experiments using parthenolide. However, we show that parthenolide does not inhibit luciferase activity *in vitro* (and thus does not seem to be toxic), and that therefore the effect observed *in vivo* should be an effect on recruitment. Although we focused on the function of TNF-α in this study, other inflammatory cytokines including IL-1β and IFN-γ also have ability to induce VCAM-1 expression in target cells (18), and may be involved in MSC accumulation.

TNF-α is a major inflammatory cytokine that plays important roles in diverse cellular events, such as cell survival, proliferation, differentiation, and death. Numerous reports have shown that TNF-α levels in serum are increased in patients with cancer (19, 20), and TNF-α is also related closely to the tumor progression including metastasis. For example, TNF-α intensely induces IL-6 and MCP-1 from cancer-associated fibroblasts and normal fibroblastic cells and has indirect influences on generation of prometastatic microenvironment (21). Furthermore, TNF-α is also released in cardiac infarction, during acute coronary syndromes, and in chronic heart failure; MSCs also accumulate at the site of cardiac infarction (22, 23). These results indicated that proinflammatory cytokines promote homing of stem cells in the heart and that these cytokines have a positive effect on cardiac regeneration. Therefore, activation with TNF-α is one of the critically important steps for MSC accumulation. Moreover, MSC-based tissue-targeted strategies may be adapted for various inflammatory diseases.

In MSC-based cancer-targeted gene therapies, it is thought that therapeutic efficacy is directly linked with accumulation efficiency of MSCs at tumor sites. Our results suggested that combination use of NF-κB inhibitors, including bortezomib, or TNF-α blocking agents, such as infliximab, reduces the

Published OnlineFirst October 12, 2012; DOI: 10.1158/0008-5472.CAN-12-0088

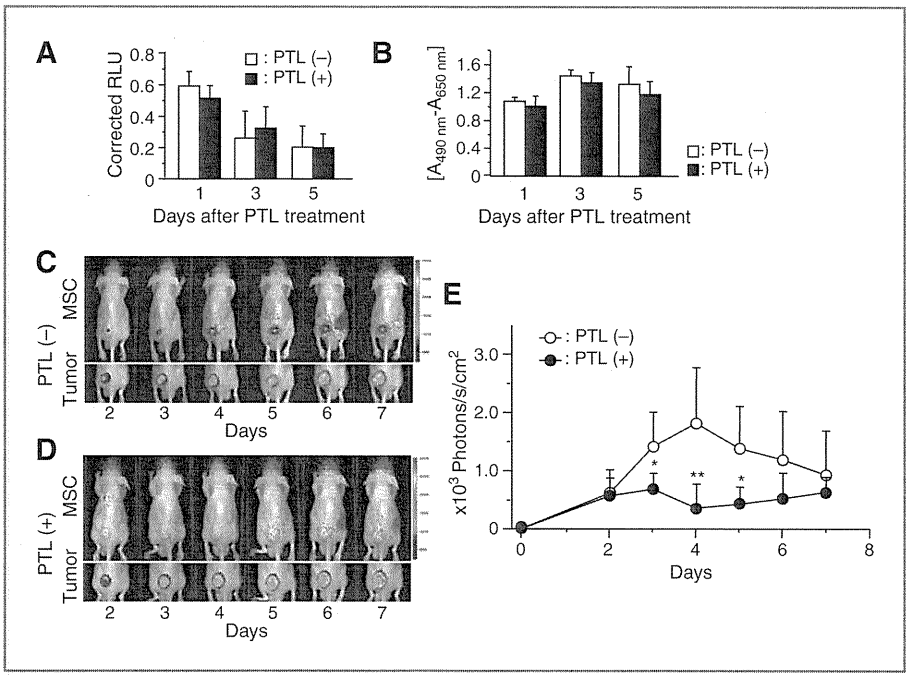

Figure 5. *In vivo* imaging of NF-κB–suppressed MSC accumulation at tumor sites. A, luciferase-expressing MSCs were cultured with parthenolide for 6 hours and luciferase assays were periodically conducted. Values are expressed as mean ± SD ($n = 4$ each). RLU, relative light unit. B, cell viability of parthenolide (PTL)-treated luciferase-expressing MSCs was also examined by XTT assays. Values are expressed as mean ± SD ($n = 4$ each). C, luciferase-expressing MSCs without parthenolide treatment were injected into tumor-bearing mice through the left ventricular cavity and IVIS imaging was periodically conducted. Each data shown are from 1 representative experiment of 8 carried out. D, luciferase-expressing MSCs with parthenolide treatment were injected into tumor-bearing mice and IVIS imaging was periodically conducted. Imaging was conducted as described earlier. Each data shown are from 1 representative experiment of 8 carried out. E, bioluminescent intensity at tumor sites was quantified using analysis software. The data are expressed as mean ± SD ($n = 8$ each). *, $P < 0.05$; **, $P < 0.01$ compared with a group of parthenolide (–) at the same time.

therapeutic efficacy of gene-modified MSCs due to inhibition of the accumulation steps. In contrast, tumor-specific TNF-α–inducing agents would be useful in enhancing therapeutic efficacy, thus further research is required in identifying such agents to more effective therapeutic strategies.

In conclusion, the present study shows that NF-κB activation through TNF-α stimulation and VCAM-1/VLA-4–mediated MSC-EC adhesion may be an important element in MSC accumulation. Although MSCs are useful as cellular vehicles for cancer-targeted gene therapy, past studies have shown that increased MSC accumulation is needed to enhance therapeutic efficacy. Thus, methodology for the enhancement of MSC accumulation should be developed and our findings suggest a solution.

Disclosure of Potential Conflicts of Interest

No potential conflicts of interest were disclosed.

Authors' Contributions

Conception and design: R. Uchibori, H. Mizukami, K. Ozawa
Development of methodology: M. Urabe
Acquisition of data (provided animals, acquired and managed patients, provided facilities, etc.): R. Uchibori
Analysis and interpretation of data (e.g., statistical analysis, biostatistics, computational analysis): R. Uchibori, H. Mizukami, A. Kume
Writing, review, and/or revision of the manuscript: R. Uchibori, M. Urabe, A. Kume
Administrative, technical, or material support (i.e., reporting or organizing data, constructing databases): T. Tsukahara, H. Mizuguchi, Y. Saga, K. Ozawa
Study supervision: M. Urabe, A. Kume, K. Ozawa

Acknowledgments

The authors thank Miyoko Mitsu for her encouragement and technical support.

Grant Support

This work was supported by Grant-in-Aid for Scientific Research (KAKENHI) from the Ministry of Education, Culture, Sports, Science and Technology (21390296 to K. Ozawa), and The Research Award to Jichi Medical School Graduate Student (to R. Uchibori).

The costs of publication of this article were defrayed in part by the payment of page charges. This article must therefore be hereby marked *advertisement* in accordance with 18 U.S.C. Section 1734 solely to indicate this fact.

Received January 13, 2012; revised August 30, 2012; accepted September 11, 2012; published OnlineFirst October 12, 2012.

References

1. Studeny M, Marini FC, Champlin RE, Zompetta C, Fidler IJ, Andreeff M. Bone marrow-derived mesenchymal stem cells as vehicles for interferon-beta delivery into tumors. Cancer Res 2002;62:3603–8.

Published OnlineFirst October 12, 2012; DOI: 10.1158/0008-5472.CAN-12-0088

2. Studeny M, Marini FC, Dembinski JL, Zompetta C, Cabreira-Hansen M, Bekele BN, et al. Mesenchymal stem cells: potential precursors for tumor stroma and targeted-delivery vehicles for anticancer agents. J Natl Cancer Inst 2004;96:1593–603.
3. Nakamizo A, Marini F, Amano T, Khan A, Studeny M, Gumin J, et al. Human bone marrow-derived mesenchymal stem cells in the treatment of gliomas. Cancer Res 2005;65:3307–18.
4. Chen X, Lin X, Zhao J, Shi W, Zhang H, Wang Y, et al. A tumor-selective biotherapy with prolonged impact on established metastases based on cytokine gene-engineered MSCs. Mol Ther 2008;16:749–56.
5. Xin H, Kanehira M, Mizuguchi H, Hayakawa T, Kikuchi T, Nukiwa T, et al. Targeted delivery of CX3CL1 to multiple lung tumors by mesenchymal stem cells. Stem Cells 2007;25:1618–26.
6. Uchibori R, Okada T, Ito T, Urabe M, Mizukami H, Kume A, et al. Retroviral vector-producing mesenchymal stem cells for targeted suicide cancer gene therapy. J Gene Med 2009;11:373–81.
7. Dwyer RM, Potter-Beirne SM, Harrington KA, Lowery AJ, Hennessy E, Murphy JM, et al. Monocyte chemotactic protein-1 secreted by primary breast tumors stimulates migration of mesenchymal stem cells. Clin Cancer Res 2007;13:5020–7.
8. Mizuguchi H, Kay MA. Efficient construction of a recombinant adenovirus vector by an improved *in vitro* ligation method. Hum Gene Ther 1998;9:2577–83.
9. Mizuguchi H, Kay MA. A simple method for constructing E1- and E1/E4-deleted recombinant adenoviral vectors. Hum Gene Ther 1999;10:2013–7.
10. Koizumi N, Mizuguchi H, Utoguchi N, Watanabe Y, Hayakawa T. Generation of fiber-modified adenovirus vectors containing heterologous peptides in both the HI loop and C terminus of the fiber knob. J Gene Med 2003;5:267–76.
11. Mittereder N, March KL, Trapnell BC. Evaluation of the concentration and bioactivity of adenovirus vectors for gene therapy. J Virol 1996;70:7498–509.
12. Coussens LM, Werb Z. Inflammation and cancer. Nature 2002;420:860–7.
13. Honczarenko M, Le Y, Swierkowski M, Ghiran I, Glodek AM, Silberstein LE. Human bone marrow stromal cells express a distinct set of biologically functional chemokine receptors. Stem Cells 2006;24:1030–41.
14. Rüster B, Göttig S, Ludwig RJ, Bistrian R, Müller S, Seifried E, et al. Mesenchymal stem cells display coordinated rolling and adhesion behavior on endothelial cells. Blood 2006;108:3938–44.
15. Butcher EC. Leukocyte-endothelial cell recognition: three (or more) steps to specificity and diversity. Cell 1991;67:1033–6.
16. Coffelt SB, Marini FC, Watson K, Zwezdaryk KJ, Dembinski JL, LaMarcad HL, et al. The pro-inflammatory peptide LL-37 promotes ovarian tumor progression through recruitment of multipotent mesenchymal stromal cells. Proc Natl Acad Sci U S A 2009;106:3806–11.
17. Zhang A, Wang Y, Ye Z, Xie H, Zhou L, Zheng S. Mechanism of TNF-α-induced migration and hepatocyte growth factor production in human mesenchymal stem cells. J Cell Biochem 2010;111:469–75.
18. Hosokawa Y, Hosokawa I, Ozaki K, Nakae H, Matsuo T. Cytokines differentially regulate ICAM-1 and VCAM-1 expression on human gingival fibroblasts. Clin Exp Immunol 2006;144:494–502.
19. Ferrajoli A, Keating MJ, Manshouri T, Giles FJ, Dey A, Estrov Z, et al. The clinical significance of tumor necrosis factor-alpha plasma level in patients having chronic lymphocytic leukemia. Blood 2002;100:1215–9.
20. Ahmed MI, Salahy EE, Fayed ST, El-Hefnawy NG, Khalifa A. Human papillomavirus infection among Egyptian females with cervical carcinoma: relationship to spontaneous apoptosis and TNF-alpha. Clin Biochem 2001;34:491–8.
21. Mueller L, von Seggern L, Schumacher J, Goumas F, Wilms C, Braun F, et al. TNF-alpha similarly induces IL-6 and MCP-1 in fibroblasts from colorectal liver metastases and normal liver fibroblasts. Biochem Biophys Res Commun 2010;397:586–91.
22. Shake JG, Gruber PJ, Baumgartner WA, Senechal G, Meyers J, Redmond JM, et al. Mesenchymal stem cell implantation in a swine myocardial infarct model: engraftment and functional effects. Ann Thorac Surg 2002;73:1919–25.
23. Pittenger MF, Martin BJ. Mesenchymal stem cells and their potential as cardiac therapeutics. Circ Res 2004;95:9–20.

Haemophilia The Official Journal of the World Federation of Hemophilia, European Association for Haemophilia and Allied Disorders and the Hemostasis & Thrombosis Research Society

Haemophilia (2014), **20**, e40–e44 DOI: 10.1111/hae.12311

ORIGINAL ARTICLE *Laboratory science*

Production of functional coagulation factor VIII from iPSCs using a lentiviral vector

Y. KASHIWAKURA,*† T. OHMORI,* J. MIMURO,* S. MADOIWA,* M. INOUE,‡ M. HASEGAWA,‡ K. OZAWA§ and Y. SAKATA*

**Research Division of Cell and Molecular Medicine, Center for Molecular Medicine, Jichi Medical University, Tochigi, Japan; †Department of Immunology, Dokkyo Medical University School of Medicine, Tochigi, Japan; ‡DNAVEC Corporation, Ibaraki, Japan; and §Division of Genetic Therapeutics, Center for Molecular Medicine, Jichi Medical University, Tochigi, Japan*

Summary. The use of induced pluripotent stem cells (iPSCs) as an autologous cell source has shed new light on cell replacement therapy with respect to the treatment of numerous hereditary disorders. We focused on the use of iPSCs for cell-based therapy of haemophilia. We generated iPSCs from mesenchymal stem cells that had been isolated from C57BL/6 mice. The mouse iPSCs were generated through the induction of four transcription factor genes Oct3/4, Klf-4, Sox-2 and c-Myc. The derived iPSCs released functional coagulation factor VIII (FVIII) following transduction with a simian immunodeficiency virus vector. The subcutaneous transplantation of iPSCs expressing FVIII into nude mice resulted in teratoma formation, and significantly increased plasma levels of FVIII. The plasma concentration of FVIII was at levels appropriate for human therapy at 2–4 weeks post transplantation. Our data suggest that iPSCs could be an attractive and prospective autologous cell source for the production of coagulation factor, and that engineered iPSCs expressing coagulation factor might provide a cell-based therapeutic strategy appropriate for haemophilia.

Keywords: haemophilia, induced pluripotent stem cells, lentiviral vector, cell therapy, gene therapy, blood coagulation

Introduction

Haemophilia is an X-linked inherited bleeding disorder, caused by mutations within the *coagulation factor VIII* (*F8*) or *coagulation factor IX* (*F9*) genes. This results in a longer than average time for blood to clot, which can lead to significant bleeding. Haemophilia is considered suitable for gene therapy, as it is caused by a single gene abnormality, and therapeutic coagulation factor levels can vary across a broad range [1]. Recently, therapeutic levels of coagulation factor have been achieved in haemophilia B patients through the direct administration of adeno-associated virus vectors in clinical trials [2]. Another gene therapy strategy for haemophilia is the application of cells transduced *ex vivo*, as a delivery vehicle for coagulation factor [3]. Cell-based therapy reduces the risk of unwanted virus dissemination, and ensures the selection of highly expressing clones prior to commencement of the procedure. However, cell-based therapies for haemophilia have been hampered in animals and during human clinical trials, because of the short life span of transplanted cells, difficulties in obtaining therapeutic plasma levels, and elimination of the transduced cells by immune reactions [4].

Induced pluripotent stem cells (iPSCs) are artificially generated stem cells, made by reprogramming somatic cells through the expression of defined transcription factors [5,6]. These iPSCs are pluripotent, with the ability to differentiate into cells of the three germ lineages *in vitro*. Mouse-derived iPSCs can be passaged through the germ line, as is the case with embryonic stem cells (ESCs). Using iPSCs has a distinct advantage over ESCs, as cells differentiated from iPSCs exhibit limited immunogenicity, and are therefore more easily tolerated by a recipient following transplantation. Accordingly, iPSC technology offers the possibility of patient-specific cell therapy for haemophilia, in which the use of genetically identical cells would prevent immune rejection. In this study, we examined whether iPSCs could release

Correspondence: Tsukasa Ohmori, MD, PhD, Research Division of Cell and Molecular Medicine, Center for Molecular Medicine, Jichi Medical University, 3111-1 Yakushiji, Shimotsuke, Tochigi 329-0498, Japan.
Tel: +81-285-58-7397; fax: +81-285-44-7817;
e-mail: tohmori@jichi.ac.jp

Accepted after revision 7 October 2013

functional coagulation factor using lentiviral transduction. We then focused on the possible clinical application of the engineered iPSCs to cell-based gene therapy for haemophilia.

Materials and methods

Mice

C57BL/6J mice were purchased from Japan SLC (Shizuoka, Japan). BALB/cAJcl-*nu/nu* mice (nude mice) were obtained from CLEA Japan, Inc. (Shizuoka, Japan). All animal procedures were approved by the Institutional Animal Care and Concern Committee at Jichi Medical University, and animal care was in accordance with the committee's guidelines.

Generation of iPSCs and cell culture

Murine mesenchymal stem cells (MSCs) were isolated and maintained as described previously [7]. We selected MSCs for the establishment of iPSCs because MSCs have a higher reprogramming efficiency compared with fibroblasts [8,9]. Two plasmid vectors to generate iPSCs (pCX-OKS-2A and pCX-cMyc) were obtained from Addgene (Cambridge, MA). MSCs were transduced with the plasmid vectors by nucleofection as described previously [10]. Colonies that were ES-like were cloned at 30 days post transduction, and MSC-derived iPSCs were maintained on mouse embryonic fibroblasts with knockout Dulbecco's modified Eagle's medium (DMEM; Invitrogen, Carlsbad, CA) supplemented with 15% foetal bovine serum, 2 mM L-glutamine, 1 mM sodium pyruvate, 0.1 mM non-essential amino acids, 0.5 mM monothioglycerol (Wako Pure Chemical Industries, Ltd., Osaka, Japan) and 1000 U mL^{-1} ESGRO (Merck Millipore, Billerica, MA).

Reverse transcription polymerase chain reaction (RT-PCR)

Total RNA was prepared using an RNeasy Mini Kit (QIAGEN, Montgomery, MD). The RT-PCR assays were conducted using a SuperScript One-Step RT-PCR System (Invitrogen). Primer pairs for the RT-PCR assays used in this study have been previously reported [5].

Lentiviral vector construct and production

The cDNA for human B-domain-deleted FVIII (hBDD-FVIII) was generated as previously described [11]. The *hBDD-FVIII* gene, under the control of a chicken β-actin promoter coupled with cytomegalovirus promoter early enhancer element (CAGp), was cloned into a self-inactivating simian immunodeficiency virus (SIV) lentiviral vector [12]. The SIV lentiviral vectors were generated as previously described [13].

Measurement of FVIII activity and antigen

The hFVIII antigens (FVIII:Ag) were measured using an anti-hFVIII-specific enzyme-linked immunosorbent assay (ELISA) kit (ASSERACHROM VIII:Ag; Diagnostica Stago, Seine, France). The functional activity of FVIII (FVIII:C) was measured using a one-stage clotting time assay on an automated coagulation analyser (Sysmex CA-500 analyser; Sysmex Corp., Kobe, Japan). We used pooled normal human plasma as a reference to measure both FVIII:C and FVIII:Ag.

Results and discussion

We first attempted to establish iPSCs from C57BL/6 mice. Bone marrow-derived MSCs were transduced with plasmid vector expressing the defined transcription factors. We cloned ESC-like cell colonies after transduction, and SSEA-1 positive cells were sorted by flow cytometry (Fig. 1a). The sorted cell colonies exhibited typical ESC morphology and alkaline phosphatase activity (Fig. 1b). The mRNA expression patterns of endogenous pluripotent-specific genes (*Sox2, Oct3/4, Nanog* and *c-Myc*) in the cells were similar to those in E14tg2a mouse ESCs (Fig. 1c). Furthermore, subcutaneous transplantation of these cells (1×10^6 cells) into nude mice resulted in the formation of teratomas containing tissues derived from the ectoderm, mesoderm, and endoderm (Fig. 1d and e). This would suggest that the cells possess the potential to differentiate into cells and tissues of the three germ layers. Therefore, we used these iPSCs for further experiments in this study.

We next examined whether iPSCs could produce functional coagulation factor after transduction by a lentiviral vector. The iPSCs were transduced with the SIV vector expressing hBDD-FVIII under the control of CAGp (SIV-CAG-hFVIII) (Fig. 2a). We cloned iPSC colonies from the cells transduced with SIV-CAG-hFVIII at a multiplicity of infection (MOI) of 30, and selected three iPSC clones that stably produced hFVIII in the supernatant (Fig. 2b). The iPSC clones expressing hFVIII were subcutaneously transplanted into nude mice. Following transplantation, plasma levels of hFVIII:Ag in nude mice gradually increased according to teratoma formation derived from the transplanted iPSCs (Fig. 2c and d). Although the plasma level of hFVIII:Ag in the nude mice was at 20%, we could not measure hFVIII:C in nude mice because of the existence of mouse FVIII. We simultaneously measured hFVIII:C and hFVIII:Ag produced from transduced

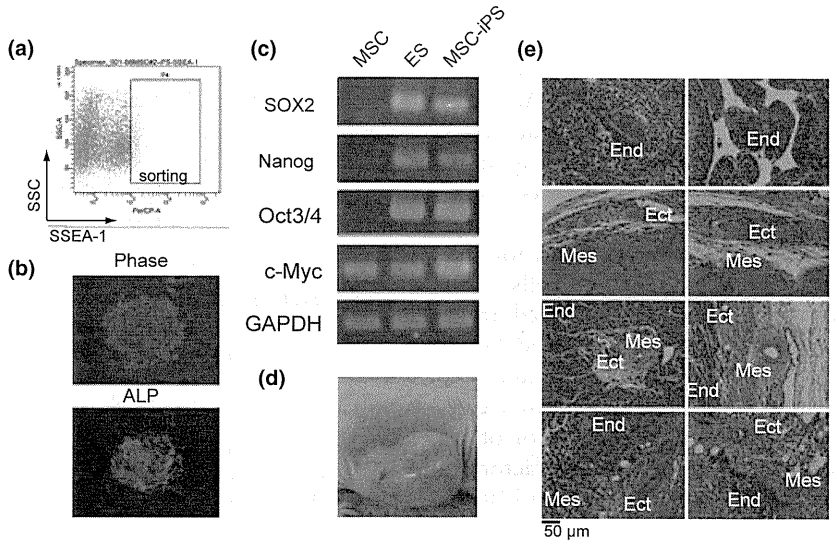

Fig. 1. Characterization of induced pluripotent stem cells (iPSCs) derived from mesenchymal stem cells (MSCs). MSCs isolated from C57BL/6 mice were transduced with plasmid vectors expressing Oc3/4, Klf4, Sox2 and c-Myc. (a) Stage-specific embryonic antigen 1 (SSEA-1) expression was examined by flow cytometry following transduction. SSEA-1-positive cells (shown in the square) were sorted as MSC-derived iPSCs. (b) Morphology of iPSC colonies derived from SSEA-1-positive cells. Alkaline phosphatase activity in iPSC colonies was detected using HNP/Fast Red TR. (c) The mRNA expression levels of the pluripotency markers SOX2, Nanog, Oct3/4 and c-Myc were determined by reverse transcription polymerase chain reaction. (d) Teratoma formation in nude mice after subcutaneous transplantation of iPSCs. (e) Differentiation into cells and tissues of the three germ lineages were confirmed by histological analysis. End, endoderm; Ect, ectoderm; Mes, mesoderm.

iPSCs, and calculated the ratio of hFVIII:C to hFVIII:Ag (0.30 ± 0.041). Accordingly, hFVIII:C levels seemed to reach the therapeutic level of FVIII required for haemophilia A (6%) in transplanted mice.

Recent studies have reported the potential of iPSCs for the treatment of many human diseases; iPSCs possess the ability to differentiate into cardiovascular [14–16], haematopoietic [16,17], neural [18], and hepatic [19,20] progenitor cells. Treatment of inherited disorders using iPSCs has been proposed for animal models of sickle cell anaemia [17]. The haemophilic mouse model could also be used to examine the potential of iPSC therapy. Xu *et al.* reported that transplantation of endothelial progenitor cells derived from iPSCs into the liver increased FVIII levels, resulting in a corrected bleeding phenotype for haemophilia A mice [21,22]. The results reported by Xu *et al.* were surprising because the differentiated endothelial progenitor cells that were transplanted only contained one copy of *F8*, yet they were able to increase plasma levels of FVIII. In contrast, lentiviral transduction using our procedure resulted in 5–10 proviral integration sites in the diploid genome at an MOI of 30, suggesting that the same procedure using engineered iPSCs expressing coagulation factor would result in a more potent therapeutic effect.

In our preliminary experiments, we used nude mice to verify the following: the net production of FVIII from iPSCs by excluding the role of the immune system; and pluripotency of iPSCs by teratoma formation. However, tumourigenesis by iPSCs, should be

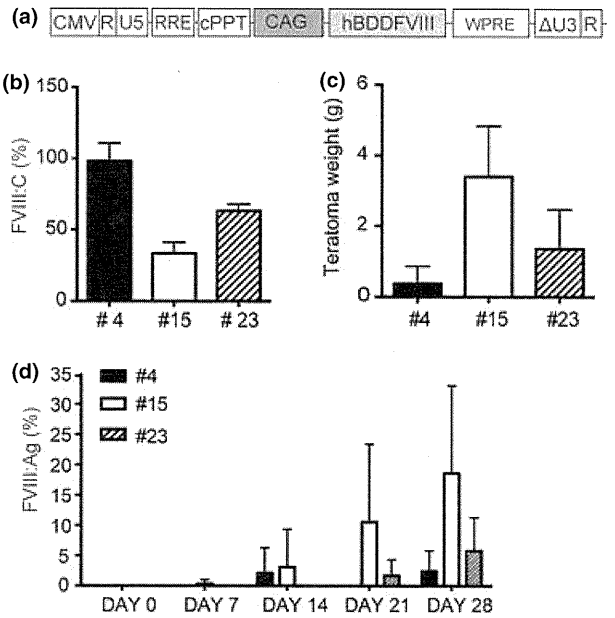

Fig. 2. Increase in FVIII levels after transduction with the simian immunodeficiency virus (SIV) lentiviral vector. The induced pluripotent stem cells (iPSCs) were transduced with SIV vector expressing human B-domain deleted coagulation factor VIII (hBDD-FVIII) under the control of a CAG promoter (SIV-CAG-hFVIII) at an MOI of 30. (a) Schematic of the SIV vectors used in our experiments. (B) FVIII activities in the supernatants derived from cloned iPSCs (#4, #15, and #23) transduced with SIV-CAG-hFVIII were measured using a one-stage clotting time assay. Values are presented as means ±SD (n = 4 for each experiment). (c, d) iPSC clones expressing hFVIII were subcutaneously transplanted into nude mice. (c) Teratoma weight at 4 weeks after subcutaneous transplantation of cloned MSC-iPSCs transduced with SIV-CAG-hFVIII. Values are presented as means ±SD (n = 3–5). (d) Plasma FVIII antigen levels in nude mice at the indicated times after subcutaneous transplantation of the iPSC clones. Values are means ±SD (n = 3–5).

completely avoided in their application. To reduce tumourigenicity and to improve the safety of iPSCs, the use of non-integrative vectors and changes of defined factors has been widely examined [6,23–25]. We also should differentiate iPSCs into the appropriate cells before transplantation, and plan to establish a more realistic cell therapy approach using immunocompetent FVIII-deficient mice.

One strategy to increase the safety of iPSCs for cell therapy would be to administer anucleated cells, such as red blood cells and platelets, differentiated from iPSCs. Integration of transgenes into genomic DNA during iPSC induction and lentiviral transduction might be negligible in the transplantation of anucleate cells. We have previously reported, along with other researchers, that expression of coagulation factor in red blood cells [26] and platelets [13,27] using lentiviral vectors has corrected the phenotype of mouse models of haemophilia. The use of blood cells to deliver coagulation factor is attractive as it avoids interference from circulating inhibitors. Recent reports have suggested the production of functional platelets from human iPSCs [28]; the transfusion of these blood cells expressing coagulation factor produced from iPSCs *in vitro* is possibly the most efficient and effective method for treating haemophiliacs.

In conclusion, we have proposed a new cell-based treatment for haemophilia involving iPSCs. Our proposed approach appears to be feasible, as transplantation of iPSCs resulted in increased and therapeutically appropriate FVIII plasma levels. Further investigations are needed to explore the risks of tumourigenicity from iPSC-derived cells, and to efficiently increase plasma levels of coagulation factor following cell therapy.

Acknowledgements

Y. Kashiwakura and T. Ohmori designed and performed the experiments, analysed the data and wrote the manuscript; M. Inoue and M. Hasegawa provided vital reagents and critically reviewed the manuscript; and J. Mimuro, S. Madoiwa, K. Ozawa and Y. Sakata analysed the data and revised the manuscript. We thank Naoko Ito and Masanori Ito (Jichi Medical University) for their technical assistance. This study was supported by a Grant from the Japan Baxter Hemophilia Scientific Research & Education Fund; Grants-in-Aid for Scientific Research (23591427, 21591249 and 23591426); Special Project Award from Bayer Hemophilia Award Program 2011; the Support Program for Strategic Research Infrastructure from the Japanese Ministry of Education and Science, and Health, Labour and Science Research Grants for Research on HIV/AIDS and Research on Intractable Diseases from the Japanese Ministry of Health, Labour and Welfare.

Disclosures

The authors stated that they had no interests that might be perceived as posing a conflict or bias.

References

1 Mannucci PM, Tuddenham EG. The hemophilias–from royal genes to gene therapy. *N Engl J Med* 2001; **344**: 1773–9.
2 Nathwani AC, Tuddenham EG, Rangarajan S *et al.* Adenovirus-associated virus vector-mediated gene transfer in hemophilia B. *N Engl J Med* 2011; **365**: 2357–65.
3 Lillicrap D, VandenDriessche T, High K. Cellular and genetic therapies for haemophilia. *Haemophilia* 2006; **12**(Suppl 3): 36–41.
4 Roth DA, Tawa NE Jr., O'Brien JM, Treco DA, Selden RF. Nonviral transfer of the gene encoding coagulation factor VIII in patients with severe hemophilia A. *N Engl J Med* 2001; **344**: 1735–42.
5 Takahashi K, Yamanaka S. Induction of pluripotent stem cells from mouse embryonic and adult fibroblast cultures by defined factors. *Cell* 2006; **126**: 663–76.
6 Okita K, Ichisaka T, Yamanaka S. Generation of germline-competent induced pluripotent stem cells. *Nature* 2007; **448**: 313–7.
7 Kashiwakura Y, Ohmori T, Mimuro J *et al.* Intra-articular injection of mesenchymal stem cells expressing coagulation factor ameliorates hemophilic arthropathy in factor VIII-deficient mice. *J Thromb Haemost* 2012; **10**: 1802–13.
8 Niibe K, Kawamura Y, Araki D *et al.* Purified mesenchymal stem cells are an efficient source for iPS cell induction. *PLoS ONE* 2011; **6**: e17610.
9 Oda Y, Yoshimura Y, Ohnishi H *et al.* Induction of pluripotent stem cells from human third molar mesenchymal stromal cells. *J Biol Chem* 2010; **285**: 29270–8.
10 Gonzalez F, Barragan Monasterio M, Tiscornia G *et al.* Generation of mouse-induced pluripotent stem cells by transient expression of a single nonviral polycistronic vector. *Proc Natl Acad Sci USA* 2009; **106**: 8918–22.
11 Ogata K, Mimuro J, Kikuchi J *et al.* Expression of human coagulation factor VIII in adipocytes transduced with the simian immunodeficiency virus agmTYO1-based vector for hemophilia A gene therapy. *Gene Ther* 2004; **11**: 253–9.
12 Nakajima T, Nakamaru K, Ido E, Terao K, Hayami M, Hasegawa M. Development of novel simian immunodeficiency virus vectors carrying a dual gene expression system. *Hum Gene Ther* 2000; **11**: 1863–74.
13 Ohmori T, Mimuro J, Takano K *et al.* Efficient expression of a transgene in platelets using simian immunodeficiency virus-based vector harboring glycoprotein Ibalpha promoter: in vivo model for platelet-targeting gene therapy. *FASEB J* 2006; **20**: 1522–4.
14 Kuzmenkin A, Liang H, Xu G *et al.* Functional characterization of cardiomyocytes derived from murine induced pluripotent stem cells in vitro. *FASEB J* 2009; **23**: 4168–80.
15 Narazaki G, Uosaki H, Teranishi M *et al.* Directed and systematic differentiation of cardiovascular cells from mouse induced pluripotent stem cells. *Circulation* 2008; **118**: 498–506.
16 Schenke-Layland K, Rhodes KE, Angelis E *et al.* Reprogrammed mouse fibroblasts differentiate into cells of the cardiovascular and hematopoietic lineages. *Stem Cells* 2008; **26**: 1537–46.
17 Hanna J, Wernig M, Markoulaki S *et al.* Treatment of sickle cell anemia mouse model with iPS cells generated from autologous skin. *Science* 2007; **318**: 1920–3.
18 Wernig M, Zhao JP, Pruszak J *et al.* Neurons derived from reprogrammed fibroblasts functionally integrate into the fetal brain and improve symptoms of rats with Parkinson's disease. *Proc Natl Acad Sci USA* 2008; **105**: 5856–61.
19 Cantz T, Bleidissel M, Stehling M, Scholer HR. In vitro differentiation of reprogrammed murine somatic cells into hepatic precursor cells. *Biol Chem* 2008; **389**: 889–96.
20 Kasuda S, Tatsumi K, Sakurai Y *et al.* Expression of coagulation factors from murine induced pluripotent stem cell-derived liver cells. *Blood Coagul Fibrinolysis* 2011; **22**: 271–9.
21 Xu D, Alipio Z, Fink LM *et al.* Phenotypic correction of murine hemophilia A using an iPS cell-based therapy. *Proc Natl Acad Sci USA* 2009; **106**: 808–13.
22 Alipio Z, Adcock DM, Waner M *et al.* Sustained factor VIII production in hemophiliac mice 1 year after engraftment with induced pluripotent stem cell-derived factor VIII producing endothelial cells. *Blood Coagul Fibrinol* 2010; **21**: 502–4.
23 Kaji K, Norrby K, Paca A, Mileikovsky M, Mohseni P, Woltjen K. Virus-free induction of pluripotency and subsequent excision of reprogramming factors. *Nature* 2009; **458**: 771–5.

24 Zhou H, Wu S, Joo JY *et al.* Generation of induced pluripotent stem cells using recombinant proteins. *Cell Stem Cell* 2009; **4**: 381–4.
25 Fusaki N, Ban H, Nishiyama A, Saeki K, Hasegawa M. Efficient induction of transgene-free human pluripotent stem cells using a vector based on Sendai virus, an RNA virus that does not integrate into the host genome. *Proc Jpn Acad Ser B Phys Biol Sci* 2009; **85**: 348–62.
26 Chang AH, Stephan MT, Sadelain M. Stem cell-derived erythroid cells mediate long-term systemic protein delivery. *Nat Biotechnol* 2006; **24**: 1017–21.
27 Shi Q, Wilcox DA, Fahs SA *et al.* Lentivirus-mediated platelet-derived factor VIII gene therapy in murine haemophilia A. *J Thromb Haemost* 2007; **5**: 352–61.
28 Takayama N, Nishimura S, Nakamura S *et al.* Transient activation of c-MYC expression is critical for efficient platelet generation from human induced pluripotent stem cells. *J Exp Med* 2010; **207**: 2817–30.

Cancer Science
Japanese Cancer Association JCA
Open Access

Novel anti-tumor mechanism of galanin receptor type 2 in head and neck squamous cell carcinoma cells

Takayuki Uehara,[1,2,3] Takeharu Kanazawa,[3,6] Hiroaki Mizukami,[2,6] Ryosuke Uchibori,[2] Tomonori Tsukahara,[2] Masashi Urabe,[2] Akihiro Kume,[2] Kiyoshi Misawa,[4] Thomas E. Carey,[5] Mikio Suzuki,[1] Keiichi Ichimura[3] and Keiya Ozawa[2,6]

[1]Department of Otorhinolaryngology, Head and Neck Surgery, Graduate School of Medicine, University of the Ryukyus, Nishihara; [2]Division of Genetic Therapeutics, Center for Molecular Medicine, Jichi Medical University, Shimotsuke; [3]Department of Otolaryngology, Head and Neck Surgery, Jichi Medical University School of Medicine, Shimotsuke; [4]Department of Otolaryngology, Head and Neck Surgery, Hamamatsu University School of Medicine, Hamamatsu, Japan; [5]Laboratory of Head and Neck Center Biology, Department of Otolaryngology, Head and Neck Surgery, The University of Michigan, Ann Arbor, Michigan, USA

Key words

Adeno-associated virus vector, Bim, extracellular signal-regulated kinases 1/2, galanin receptor, head and neck squamous cell carcinoma

Correspondence

Takeharu Kanazawa, Department of Otolaryngology, Head and Neck Surgery, Jichi Medical University School of Medicine, 3311-1 Yakushiji, Shimotsuke 329-0498, Japan.
Tel: 0285-58-7381; Fax: 0285-44-5547;
E-mail: kanatake@omiya.jichi.ac.jp

[6]These three authors made an equal contribution towards the conduct and reporting of this study.

Funding information

Ministry of Education, Culture, Sports, Science, and Technology of Japan (22591916, 23592539)

Received June 25, 2013; Revised October 23, 2013; Accepted October 27, 2013

Cancer Sci **105** (2014) 72–80

doi: 10.1111/cas.12315

Galanin and its receptors, GALR1 and GALR2, are known tumor suppressors and potential therapeutic targets in head and neck squamous cell carcinoma (HNSCC). Previously, we demonstrated that, in GALR1-expressing HNSCC cells, the addition of galanin suppressed tumor proliferation via upregulation of ERK1/2 and cyclin-dependent kinase inhibitors, whereas, in GALR2-expressing cells, the addition of galanin not only suppressed proliferation, but also induced apoptosis. In this study, we first transduced HEp-2 and KB cell lines using a recombinant adeno-associated virus (rAAV)-green fluorescent protein (GFP) vector and confirmed a high GFP expression rate (>90%) in both cell lines at the standard vector dose. Next, we demonstrated that GALR2 expression in the presence of galanin suppressed cell viability to 40–60% after 72 h in both cell lines. Additionally, the annexin V-positive rate and sub-G0/G1 phase population were significantly elevated in HEp-2 cells (mock *vs* GALR2: 12.3 *vs* 25.0% ($P < 0.01$) and 9.1 *vs* 32.0% ($P < 0.05$), respectively) after 48 h. These changes were also observed in KB cells, although to a lesser extent. Furthermore, in HEp-2 cells, GALR2-mediated apoptosis was caspase-independent, involving downregulation of ERK1/2, followed by induction of the pro-apoptotic Bcl-2 protein, Bim. These results illustrate that transient GALR2 expression in the presence of galanin induces apoptosis via diverse pathways and serves as a platform for suicide gene therapy against HNSCC.

Head and neck squamous cell carcinoma (HNSCC) is diagnosed in more than 500 000 patients worldwide each year, accounting for 5% of all malignancies.[1,2] Despite multidisciplinary therapy, the prognosis of patients with advanced HNSCC has remained poor over several decades.[3] Thus, the invention of new therapeutic approaches against HNSCC, such as gene therapy and molecular targeted therapies has received much attention.[4–7] However, these novel treatments remain inadequate, because various signal transduction systems are defective in typical HNSCC, and little therapeutic effect is achieved by therapies targeting single mechanisms. Thus, there is a need to develop an effective drug delivery system and a novel molecular targeted therapy with multiple therapeutic targets.

In general, tyrosine kinase receptors and cytokine receptors, and their signaling pathways are important in carcinogenesis[5,8] and they have been analyzed as molecular targets and prognostic factors in HNSCC. However, the roles of G-protein–coupled receptors (GPCRs), which are important signaling molecules, are not fully understood. GPCRs control various signaling pathways in all tissues of the body, and approximately 30% of all current pharmaceuticals exert their therapeutic effects by interacting with GPCRs. Therefore, the field of GPCRs holds promise for further drug discovery and therapeutic development.[9]

Previously, we investigated the function and signal transduction of galanin receptors, which are representative GPCRs in HNSCC.[10,11] Galanin is a 30-amino acid peptide, which has three specific receptors (GALR1–3). Galanin and its receptors are mainly expressed in the central and peripheral nervous systems and function in neurotransmission.[12–14] Recently, galanin has been shown to regulate cell proliferation and survival in many tumors.[15–17] With the development of functional analysis methods for each receptor, it became clear that GALR1 and GALR2 are likely to act as tumor suppressors. Our previous study showed that activation of the GALR1 signaling pathway suppressed tumor cell proliferation via phosphorylation of ERK1/2, and involves upregulation of the cyclin-dependent kinase inhibitors in HNSCC.[10,18] Other studies showed that GALR1 inhibits proliferation by inactivat-

ing the mitogen-activated protein kinase (MAPK) pathway in oral carcinoma.[19] Moreover, activation of the GALR2 signaling pathway suppresses tumor cell growth through induction of apoptosis in some tumors, including HNSCC.[11,20,21] The cytotoxic effects of the GALR2 signaling pathway are partially mediated by dephosphorylation of Akt and the Bcl-2 protein, Bad, in PC12 cells, a pheochromocytoma cell line.[21]

However, further analysis is required with respect to prognostic factors in HNSCC, applications of molecular targeted therapy, and clinical applications of gene therapy. The adeno-associated (AAV) vector is a promising system in gene therapy, holding various benefits, such as a lack of pathogenicity, low immunogenicity, long-term transgene expression, and broad tissue-specificity.[22,23] To date, AAV vectors have been used in clinical trials for the treatment of various diseases, such as Parkinson's disease, hemophilia B, and inherited retinal disorders.[24–27] Additionally, it is thought to be applicable to suicide-gene therapy against various cancers, including HNSCC.[28–30] rAAV-galanin is currently clinically applied in the suppression of limbic seizure activity,[31] and this vector is suitable for use in the galanin–GALR system. Given this background, we set out to evaluate the effects of GALR expression on apoptosis and analyzed the associated mechanism of action using HNSCC cells.

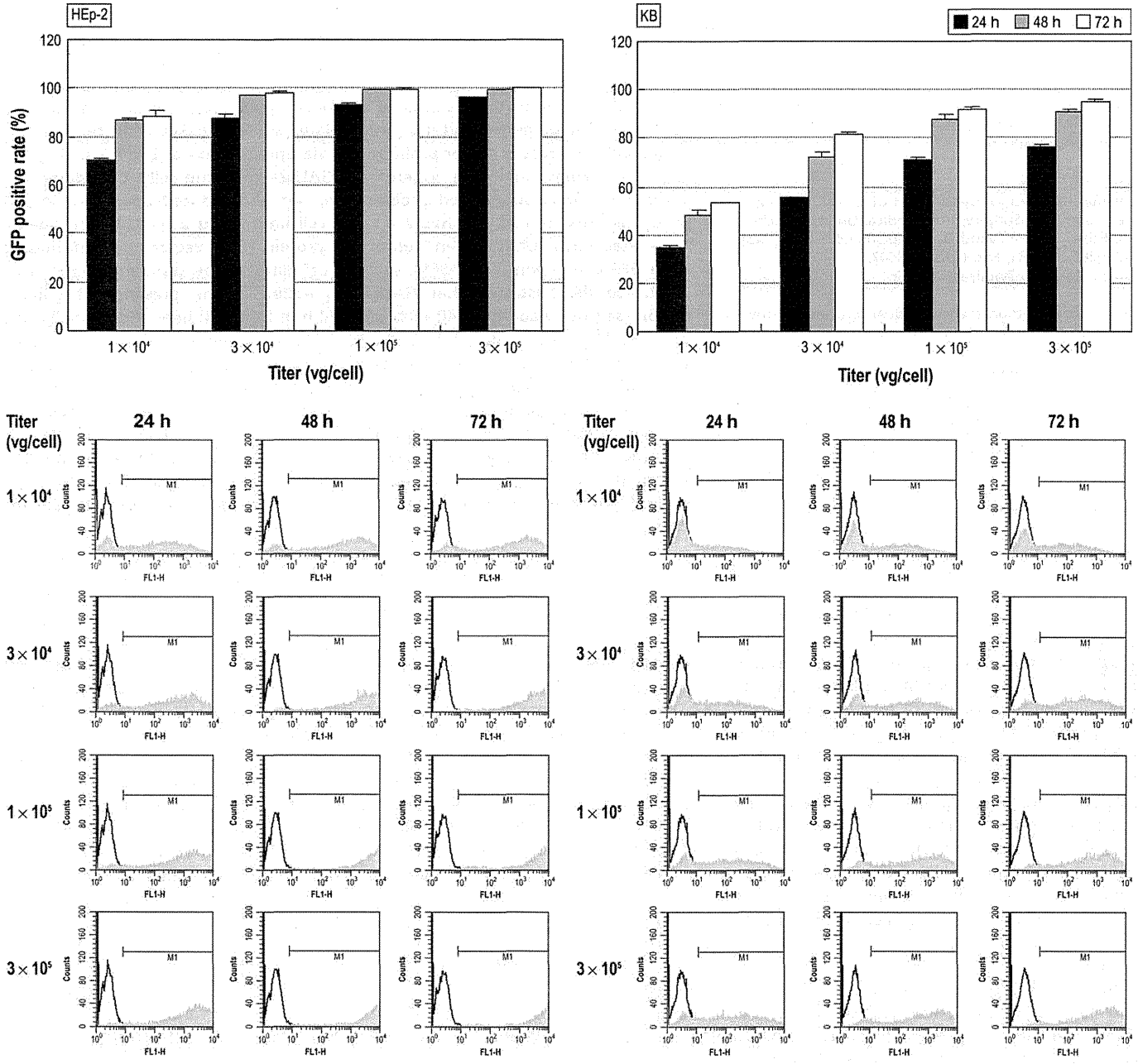

Fig. 1. Transduction efficiency using recombinant adeno-associated virus (rAAV)-enhanced green fluorescent protein (EGFP) in head and neck squamous cell carcinoma (HNSCC) cell lines. HEp-2 and KB cells were transduced by AAV-EGFP at various vector doses. *Upper*: GFP-positive cell rate under vector dose-dependent and time-course conditions in each cell line are indicated. *Lower*: Raw data expressing GFP intensity as a measure of gene expression.

Material and Methods

Cell culture and reagents. Human laryngeal carcinoma cell line HEp-2 and human oral carcinoma cell line KB were purchased from American Type Culture Collection (Manassas, VA, USA). Cells were cultured in αMEM (Gibco, Grand Island, NY, USA) supplemented with 10% heat-inactivated fetal bovine serum, 100 U/mL penicillin, and 100 μg/mL streptomycin. Human galanin was obtained from ANASPEC (San Jose, CA, USA), PD98059 and staurosporine from Wako (Osaka, Japan), and z-VAD-fmk from Promega (Madison, WI, USA). Although KB cells were originally thought to be derived from an epidermal carcinoma of the mouth, HeLa cell contamination was found thereafter through isoenzyme and other analyses (http://www.atcc.org/Products/All/CCL-17.aspx). Therefore, KB cells may not be a pure HNSCC cell line. However, we used both cell lines to understand the universal function of GALR2, rather than its cell-specific function.

Plasmid and rAAV vector production. The GALR1HA-Ires-GFP and GALR2HA-Ires-GFP fragments were obtained from our previous experiments.[10] The sequences were subcloned into the pAAV-MCS vector (Agilent technologies, Palo Alto, CA, USA).

To produce recombinant AAV vectors, we used an AAV helper-free system (Agilent technologies). Each pAAV vector, pAAV-RC, and the pHelper plasmid were cotransfected into subconfluent HEK293 cells by the calcium phosphate precipitation method or by polyethylenimine. After 72-h incubation, cells were harvested and lysed using three freeze-thaw cycles. The crude viral lysate was purified by two rounds of CsCl density-gradient ultracentrifugation. The titer of rAAV vectors was subsequently determined by quantitative PCR analysis.

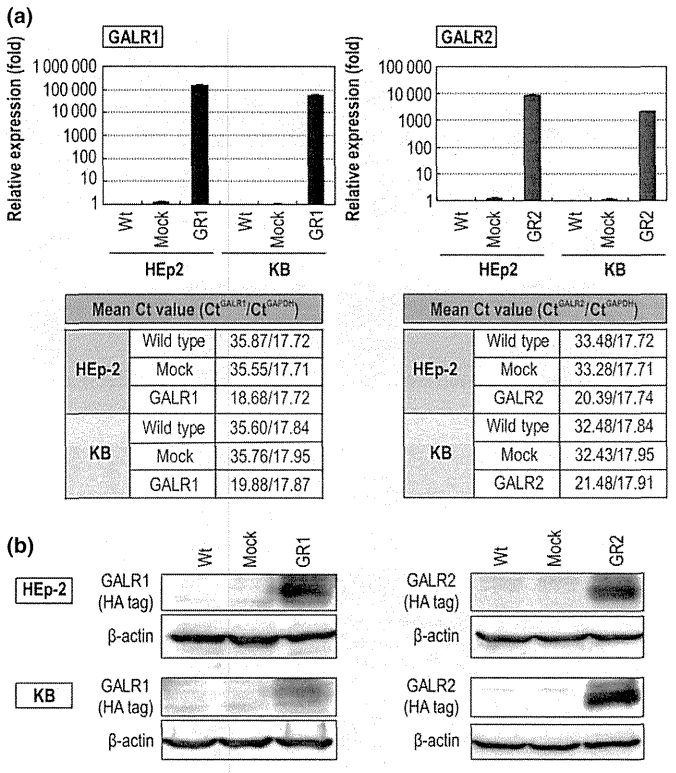

Fig. 2. Expression of GALR1 and GALR2 using individual recombinant AAV vectors in head and neck squamous cell carcinoma (HNSCC) cells. (a) Quantitative RT-PCR was performed to measure GALR1 and GALR2 expression in wild type (Wt) or HNSCC cells transduced by each of the rAAV vectors. (b) Western blot results showing exogenous GALR1 and GALR2 expression in Wt or HNSCC cells transduced by each of the rAAV vectors, as detected by an HA-antibody.

Quantitative RT-PCR. Total RNA was isolated using an RNeasy mini kit (Qiagen, Valencia, CA, USA). Reverse transcription was performed using a High Capacity cDNA Reverse Transcription Kit (Applied Biosystems, Foster City, CA, USA) according to the manufacturer's protocol. cDNA was amplified using TaqMan Expression Assays (Applied Biosystems): GalR1 (Hs00175668 m1), GalR2 (Hs00605839 m1), and GAPDH (Hs99999905 m1). The PCR conditions were as follows: 50°C for 2 min, 95°C for 10 min, and 40 cycles each consisting of 95°C for 15 s and 60°C for 1 min. The expression levels of the target genes were analyzed using the comparative C_t method, and GAPDH was used as a control gene.

Immunoblotting. Cells were lysed in a buffer containing 62.5 mM Tris-HCl (pH6.8), 2% SDS, 10% glycerol, 6% mercaptoethanol, and 0.01% bromophenol blue. To detect GALRs expression, cell lysates were treated with N-Glycosidase F (New England BioLabs, Beverley, MA, USA) without boiling, as described previously.[10,11] Mitochondrial and cytosolic fractions were obtained using Mitochondrial Isolation Kit (ThermoFisher Scientific, Logan, UT, USA).

Samples were gel electrophoresed and transferred to polyvinylidene difluoride membranes, which were probed with specific antibodies. Mouse monoclonal antibodies to hemagglutinin (HA)-tag, phospho-Bad (Ser112), and β-actin, rabbit monoclonal antibodies to p44/42 MAPK (Erk1/2), phospho-p44/42 (Thr202/Tyr204), Akt, phospho-Akt, caspase-3, cleaved caspase-3, Bax, Bcl-2, Bcl-xL, Mcl-1, Bim, Bad, survivin, antibodies to Cox IV and XIAP, polyclonal antibodies to AIF, Endonuclease G, Bit1, HtrA2 and cytochrome c were purchased from Cell Signaling Technology (Beverly, MA, USA). Bands were visualized using an Enhanced Chemiluminescence Kit (GE Healthcare, Buckinghamshire, UK) and an ImageQuant LAS 4000 (Fujifilm, Tokyo, Japan).

Immunocytochemistry. Cells were seeded onto coverslips and incubated overnight, and transduced with each recombinant AAV vector. After 48 h of incubation, cells were fixed, and stained with mouse monoclonal anti-HA-tag antibody (Cell Signaling). Subsequently, cells were stained with Alexa Fluor 555-labeled goat anti-mouse IgG (Cell Signaling) and the nuclei counterstained with DAPI. Furthermore, to determine the transport potential of HA-tagged GALRs proteins to the cytoplasmic membrane, HEp-2 cells stably expressing these proteins were established by transfecting the AAV plasmid into HEp-2 cells using Lipofectamine (Invitrogen, Carlsbad, CA, USA). Green fluorescent protein-positive cells were selected by flow cytometry using a FACS Vantage SE at 4 weeks after transfection (BD Biosciences, San Diego, CA, USA). Exogenous GALR1 or GALR2 were localized using a BIOREVO BZ-9000 microscope (Keyence, Osaka, Japan) and an Olympus FV-500 Confocal Microscope (Olympus Corporation, Tokyo, Japan).

Cell viability assay. The effect of activation of the GALR signaling pathways on cell viability was examined using WST-1 (Roche Diagnostics, East Sussex, UK). Cells were seeded in a 96-well microculture plate, incubated overnight, and then cultured in serum-free media (SFM) containing 0.1% bovine serum albumin for 2 h. Subsequently, cells were exposed to the individual rAAV vectors and galanin for 24–72 h. WST-1 reagent was added for the last 1–2 h of the incubation, and the absorbance at 450 nm was measured

using a Spectra Max 190 microplate reader (Molecular Devices, Sunnyvale, CA, USA).

Apoptosis and cell cycle analysis. Apoptotic cells were detected by staining with phycoerythrin (PE)-conjugated annexin V protein (BD Bioscience, San Jose, CA, USA) and flow cytometry. Cell cycle analysis was performed with the CycleTEST PLUS DNA Reagent Kit (BD Biosciences) and flow cytometry. Apoptosis-induced DNA fragmentation was measured for the sub-G0/G1 cell cycle phase populations.

Statistical analysis. Statistical analysis was performed using Student's *t*-test and Kruskal–Wallis test.

Results

Transduction efficiency of HNSCC cell lines using rAAV-EGFP. To determine transduction efficiency in HNSCC cell lines using rAAV vectors, HEp-2 and KB cells were infected with a rAAV-EGFP vector at various vector doses. After incubation for 24–72 h, GFP-positive cells were counted by flow cytometry. We confirmed a high GFP expression (>90%) in both HNSCC cell lines transduced by vector doses above 1×10^5 vector genomes (vg)/cell for 48 h (Fig. 1). Consequently, a titer of 1×10^5 vg/cell was used as standard vector dose.

GALR gene expression after transduction of rAAV-GALR vectors. We determined both the endogenous and exogenous mRNA expression levels of each GALR gene in HEp-2 and KB cells transduced by rAAV-GALR1 or rAAV-GALR2 by quantitative RT-PCR. After 48 h of transduction, elevated mRNA expression levels of exogenous GALR1 and GALR2 were observed in both cell lines (Fig. 2a).

The expression levels of exogenous GALR1 and GALR2 proteins were also assessed by western blot analysis and immunocytochemistry, using a mouse monoclonal anti-HA tag antibody, and confirmed robust expression of GALR1 and GALR2 proteins (Figs 2b,3). Immunofluorescence revealed that GFP-positive cells showed exogenous expression of GALRs, which was localized to both the cytoplasm and plasma membrane in cells transiently transduced with AAV vectors (Fig. 3a). However, in stable GALRs-expressing HEp-2 cells, exogenous GALRs located only to the plasma membrane (Fig. 3b). These results suggested that transient-transduction impelled movement of a large quantity of these proteins to the cytoplasm, although these proteins themselves have the potential to be transported to the plasma membrane, as expected for a G protein-coupled receptor.

Co-administration of rAAV-GALR2 and galanin inhibits cell proliferation and induces apoptosis. We examined the ability of each GALR signaling pathway to inhibit HNSCC growth. Culture of cells in the presence of both rAAV-GALR2 and varying doses of galanin in SFM for 24–72 h resulted in cell growth suppression in a time- and dose-dependent manner in both HNSCC lines, as assessed by WST-1 assay. After 72 h of stimulation, the cell growth rate was significantly decreased to 40% in HEp-2 and 60% in KB cells (Fig. 4a). In contrast,

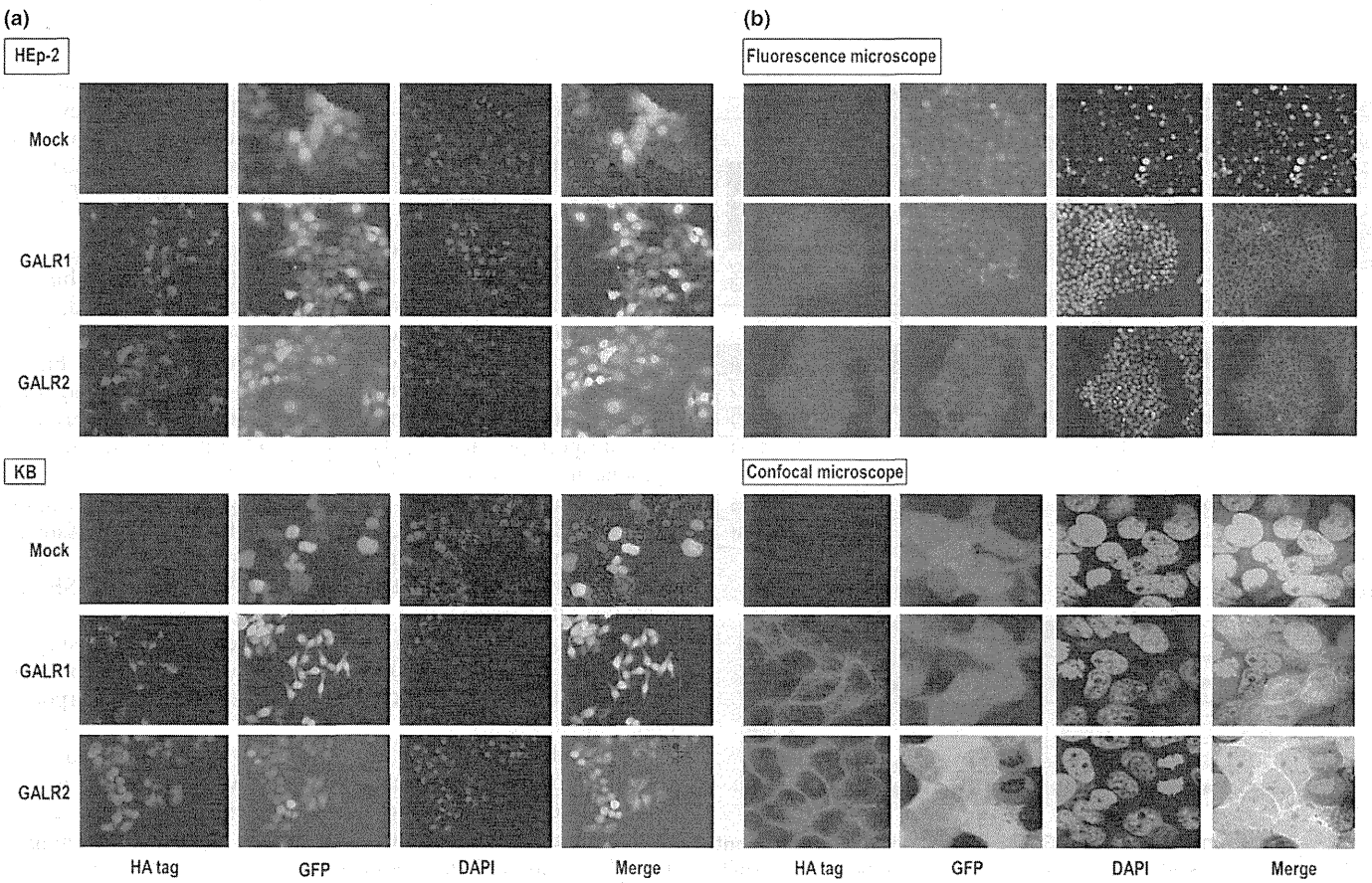

Fig. 3. (a) Exogenous GALR1 and GALR2 localization in head and neck squamous cell carcinoma (HNSCC) cells transiently transduced with each of the recombinant adeno-associated virus (rAAV) vectors. (b) Exogenous GALR1 and GALR2 localization in HEp-2 cells stably transfected with each of the AAV plasmids. Images show cells stained with the anti-HA antibody (left-most), green fluorescent protein (GFP) (second from the left), DAPI (4′6′-diamidino-2-phenylindole dihydrochloride) (second from the right), and merged images (right-most).

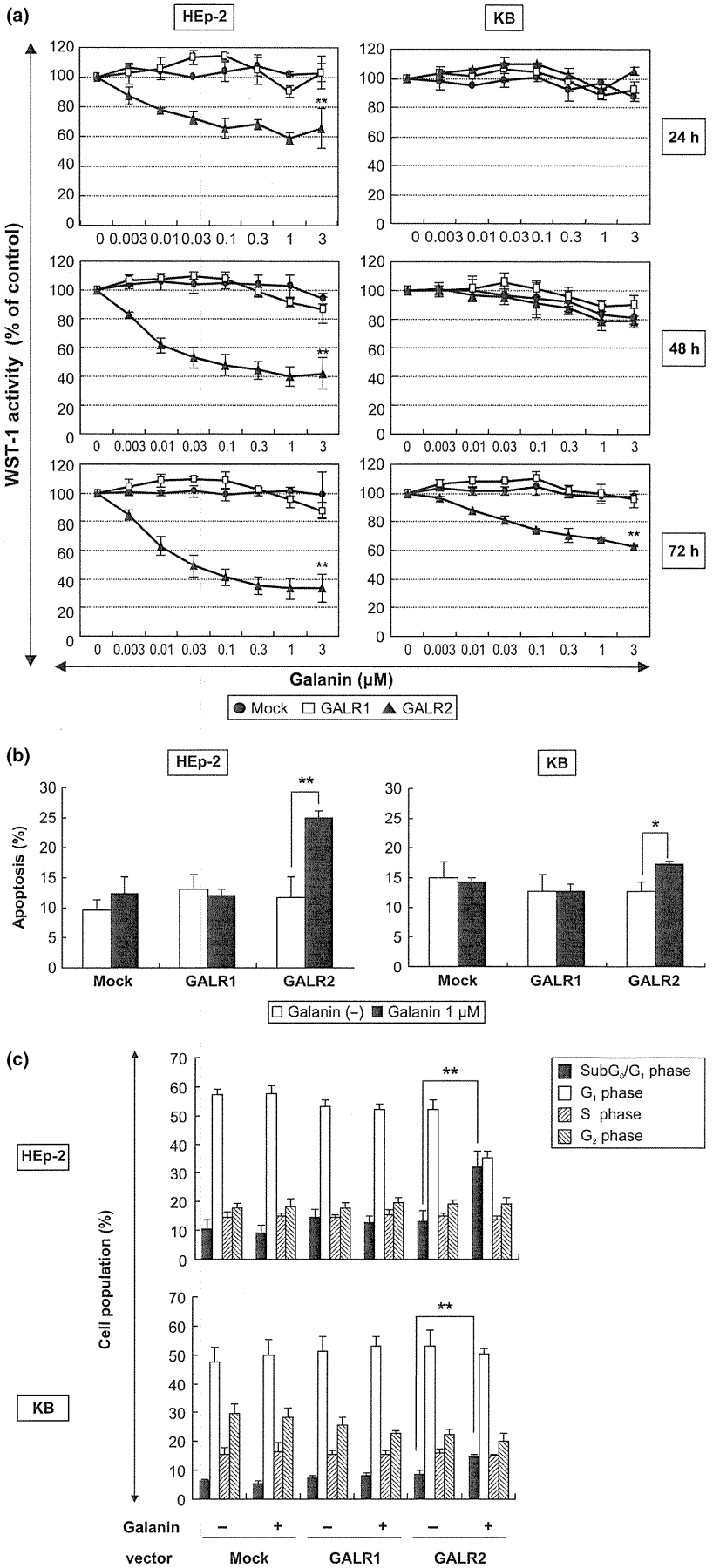

Fig. 4. Co-administration of galanin and recombinant adeno-associated virus (rAAV)-GALR2 during cell culture inhibited cell proliferation and induced cell death in head and neck squamous cell carcinoma (HNSCC) cells. (a) Inhibitory effects of galanin on growth of HNSCC cells transduced with the respective rAAV vectors. (b) Flow cytometric analysis of cell apoptosis using the annexin V. (c) Cell cycle analysis by flow cytometry. $^{*}P < 0.05$; $^{**}P < 0.01$.